

Contract No:

This document was prepared in conjunction with work accomplished under Contract No. DE-AC09-08SR22470 with the U.S. Department of Energy (DOE) Office of Environmental Management (EM).

Disclaimer:

This work was prepared under an agreement with and funded by the U.S. Government. Neither the U. S. Government or its employees, nor any of its contractors, subcontractors or their employees, makes any express or implied:

- 1) warranty or assumes any legal liability for the accuracy, completeness, or for the use or results of such use of any information, product, or process disclosed; or
- 2) representation that such use or results of such use would not infringe privately owned rights; or
- 3) endorsement or recommendation of any specifically identified commercial product, process, or service.

Any views and opinions of authors expressed in this work do not necessarily state or reflect those of the United States Government, or its contractors, or subcontractors.

Project Title: Low-Cost Metal Hydride Thermal Energy Storage System for Concentrating Solar Power Systems

Project Period: 10/01/12 – 1/31/16

Project Budget: \$ 1,873,333

Submission Date: 1/31/16

Recipient: Savannah River National Laboratory

Address: Bldg. 999-2W
Aiken, SC 29808

Award Number: SRNL_Zidan_A

Project Team: Savannah River National Laboratory and Curtin University

Contacts: Ted Motyka
Project Manager and Co-PI
Phone: 803-507-8548
Email: ted.motyka@srnl.doe.gov

Ragaiy Zidan
Lead-PI
Phone: 803-646-8876
Email: ragaiy.zidan@srnl.doe.gov

TABLE OF CONTENTS

Executive Summary.....	1
1.0 Introduction.....	3
1.1 Background.....	3
1.2 Objective.....	3
1.3 Approach.....	3
2.0 Project Results and Discussion.....	4
2.1 Material Property Data Generation and Material Modifications.....	4
2.1.1 Preliminary Material Engineering Data.....	4
2.1.1.1 High Temperature Material Synthesis and Material Evaluation.....	5
2.1.1.2 Low Temperature Material Evaluation and Performance	8
2.1.2 Modify and Engineer MH Materials to Meet SunShot Targets.....	11
2.1.2.1 High Temperature Material Synthesis and Material Evaluation.....	12
2.1.2.2 Low Temperature Material Evaluation and Performance	15
2.2 Screening Tool, Cost and Performance Modeling, and Application.....	16
2.2.1 Development and Evaluation of Screening Tools.....	16
2.2.2 Development and Evaluation of Transport and System MH TES Models....	26
2.3 Design and Testing of a Bench-Scale MH TES System.....	41
2.3.1 Design and Fabrication of a Bench-Scale MH TES System.....	42
2.3.2 Operation of a Bench-Scale MH TES System.....	43
3.0 Project Summary and Conclusions.....	44
3.1 Milestones and Accomplishments.....	44
3.2 Path Forward.....	46
4.0 References.....	46

Low-Cost Metal Hydride Thermal Energy Storage System for Concentrating Solar Power Systems

**R. Zidan, B. J. Hardy, C. Corgnale, J. A. Teprovich
P. Ward, and T. Motyka**
Savannah River National Laboratory
Aiken, SC, 29808

Executive Summary

The objective of this research was to evaluate and demonstrate a metal hydride-based TES system for use with a CSP system. A unique approach has been applied to this project that combines our modeling experience with the extensive material knowledge and expertise at both SRNL and Curtin University (CU). The major task objectives for the overall project are listed below in Table 1. A brief summary of the accomplishments for all 3 project periods are described below.

Table 1: Project Major Tasks

SRNL CSP MH TES Project Major Task Objectives	
Period	TASKS
1.1	Obtain and generate preliminary material engineering data
1.2	Refine and apply material screening tool (Preliminary System Models)
1.3	Design and fabricate a bench-scale MH TES system
2.1	Modify and engineer MH materials to meet DOE Sunshot targets
2.2	Generate detailed engineering property data for modified materials
2.3	Develop and evaluate transport and system MHTES models
3.1	Operate bench-scale MH TES
3.2	Obtain detailed engineering property data on the final selected MH materials that best meet DOE targets

Period 1 - SRNL and CU collected and evaluated material property data for over 20 MH candidates. From these materials three potential pairs of materials were selected as the most promising materials capable of meeting many of the DOE SunShot targets. These material pair included: 1) $Mg_2Fe_3H_6/NaMgH_3-NaAlH_4$ (SAH), 2) $TiH_{1.72} - TiXY$ and 3) $CaH_2 - TiXY$ (where X & Y are typically Fe, Mn). Even though the selected material pairs showed excellent potential for CSP TES applications, our preliminary techno-economic analysis showed that none of the existing pairs of materials could meet all of the DOE targets.

Period 2 – Therefore, the major objective of Period 2 was to modify these materials to enhance their TES performance to meet all the targets. For the HTMH materials SRNL and CU concentrated on 3 main material modifications. A fluoride modified sodium magnesium material ($NaMgH_2F$) that not only lowers cost and raises operating temperatures but also was expected to minimize the evaporation and deposition of Mg that was found to occur at higher temperatures. The other two modifications involved changes to the higher temperature Ti and Ca materials.

Modification to the Ti system examined alloying Ti with Al to help lower the cost of the material. Recent attempts to modify CaH_2 , which is a very high temperature and a very low cost hydride material, resulted in the development of a new process patent by SRNL [1]. The new process was shown to have the potential to create a HTMH material that is not only low cost and high temperature but also mitigates unwanted material melting and evaporation. For the LTMH material pairing the hexahydride form of SAH (Na_3AlH_6) was identified and evaluated as an improved alternative to SAH that operates at lower pressure and has better cycling stability.

During Project Period 2, thermodynamic and cycling data was collected for the above modified material pairs and was provided to the modeling team. A comparison between the performance of the newly developed materials and previously identified ideal MH materials was carried out using the general methodology that will be described in more detail later in this report. Also during Period 2, a finite element heat and mass transport model was developed that predicts the transient behavior of these parameters for the bench-scale and prototype test systems. A higher level system model was developed for evaluating the overall performance of various metal hydride TES configurations along with inputs and outputs from various solar collectors and power generators. The model was used to compare the techno-economic performance of the MH based TES system against other available systems.

Period 3 – The thermal and kinetic properties of the most promising modified materials were measured including enthalpy, entropy, bulk density, hydrogen capacity, activation energy, thermal conductivity and cycling stability. This included the new low cost metal hydride capable of reversibly storing ~ 2-2.5 wt. % hydrogen at 700-750 °C. This material is currently the most promising high temperature metal hydride material discovered for TES applications capable of meeting DOE cost targets.

A bench-scale cycling apparatus was operated to demonstrate the cycling of hydrogen between the two hydride beds. The detailed MH model developed in Period 2 was used to simulate the behavior of the selected modified LTMH material (Na_3AlH_6) and to compare the obtained results with the experimental results, showing very good agreement with temperature and pressure profiles. In addition, the MH pair MgFe_2H_6 - Na_3AlH_6 was examined and modeled using the previously developed system model. Results showed that the two materials can successfully be paired under selected experimental conditions and properties.

1. Introduction

1.1. Background

Three of the major improvement areas for Thermal Energy Storage (TES) systems are in 1) lowering their costs, 2) reducing their full charging time to less than 6 hours and 3) increasing their temperature of operation to improve the CSP overall production efficiency. Metal hydride TES systems have the ability to enable all of these improvements. In addition, many of the high and even the new lower temperature metal hydrides are fairly inexpensive. Preliminary calculations indicate that existing metal hydride TES systems can approach \$15-\$25/kWh. Because of their very high thermal capacity (approximately 15-20 times that of current systems), the size of the overall TES systems along with its associated BOP can be substantially reduced leading to additional capital cost savings. Metal hydride TES systems can also be made to be self-regulating, thereby simplifying their design and lowering not only their capital but their operating costs as well.

1.2 Objective

The objectives of this research are to evaluate and demonstrate a metal hydride-based TES system for use with a CSP system. Because of their high energy capacity and reasonable kinetics many metal hydride systems can be charged rapidly. Metal hydrides for vehicle applications have demonstrated charging rates in minutes and tens of minutes as opposed to hours. This coupled with high heat of reaction allows metal hydride TES systems to produce very high thermal power rates (approx. 1kW per 6-8 kg of material). A major objective of this work is to evaluate some of the new metal hydride materials that have recently become available. A problem with metal hydride TES systems in the past has been selecting a suitable high capacity low temperature metal hydride material to pair with the high temperature material. A unique aspect of metal hydride TES systems is that many of these systems can be located on or near dish/engine collectors due to their high thermal capacity and small size. The primary objective of this work is to develop a high enthalpy metal hydride that is capable of reversibly storing hydrogen at high temperatures ($> 650\text{ }^{\circ}\text{C}$) and that can be paired with a suitable low enthalpy metal hydride with low cost materials. Furthermore, a demonstration of hydrogen cycling between the two hydride beds is desired.

1.3 Approach

A unique approach is being applied to this project that makes use of the hierarchal modeling methodology developed by the Savannah River National Laboratory (SRNL) [2]. This approach combines our modeling experience with the extensive material knowledge and expertise at both SRNL and Curtin University (CU) to screen several promising metal hydride candidate materials and then select the best candidates for more thorough evaluation through experiments and more detailed models. During this three-year project, a newly developed high temperature metal hydride was developed and characterized. A bench-scale, hydrogen cycling TES system was constructed and tested as a proof of concept for this technology. This research project then integrated the experimental results into a design of a metal

hydride energy storage system aimed at demonstrating the technology and development of a material capable of meeting the SunShot cost and performance targets for TES systems. The development of this technology will allow CSP systems to further expand their role in the renewable energy marketplace.

2. Project Results and Discussion

During the course of this project numerous metal hydride materials were evaluated as potential thermal energy storage candidates. This investigation determined the key material properties including: hydrogen capacity, cycling stability, enthalpy, entropy, density, kinetics, thermal conductivity, and activation energy for a wide variety of metal hydrides and modified metal hydride composite materials. In depth cost analysis and system modeling calculations were also performed in tandem to provide direction and feasibility for the investigated materials. This project has resulted in the realization of a new class of materials which are both low in cost and able to operate at temperatures (> 650 °C) desired for high efficiency thermal energy storage systems for CSP applications.

2.1 Material Property Data Generation and Material Modifications

SRNL focused on the development and modification of low-cost materials for thermal energy storage application during the course of this project. As part of the material evaluation process, the thermodynamic and kinetic properties for numerous materials and modified materials were acquired. Modifications to materials, such as the addition of catalysts, thermal conduction enhancing materials, and stabilizing agents were explored to develop suitable metal hydride materials.

2.1.1 Preliminary Material Engineering Data

The experimental material properties for several known metal hydride materials were evaluated for suitability as metal hydride thermal energy storage pairs. During the evaluation it was discovered that many of the well-known metal hydrides were either too expensive, the operating temperature was lower than desired, or the equilibrium pressures were not sufficient. The first year of this project evaluated a large array of known materials for potential candidates with no material pair quite reaching the desired targets [3]. It was apparent that material modification and new material synthesis would be required to produce materials capable of reaching Sunshot targets. Figure 1 below provides operational pressure and temperature conditions for some of the materials which were considered.

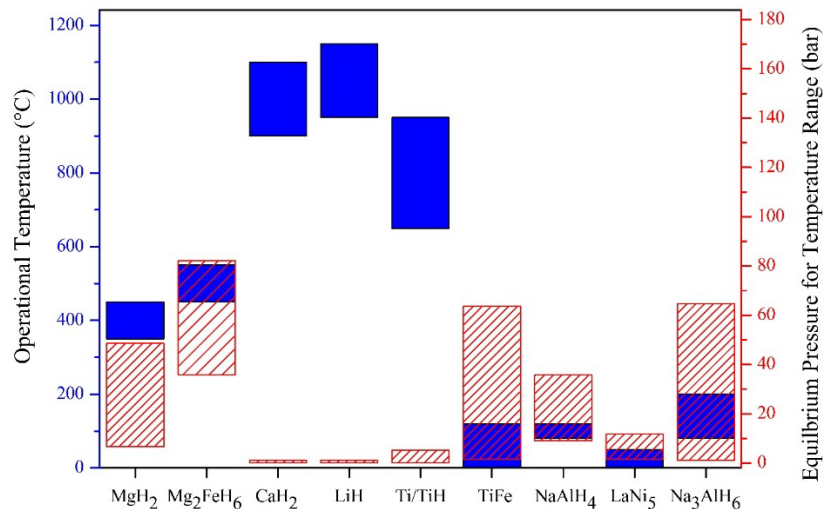


Figure 1: Operational temperature range for various low and high enthalpy metal hydrides (solid blue bar) and their corresponding hydrogen equilibrium pressure range (dashed red bar).

2.1.1.1 High Temperature Material Synthesis and Material Evaluation

Mg_2FeH_6 was investigated as a high temperature metal hydride material for TES applications. This material was known to have a high enthalpy, reasonable cycle stability, and fast kinetics. This material was found to be far more ideal for TES applications than MgH_2 . SRNL produced results from Kissinger plots that indicate a decrease in the activation energy (E_a) required for desorption compared to those of MgH_2 and Mg_2FeH_6 found in the literature (Figure 2). An activation energy (E_a) of 89.5 ± 0.9 kJ/mol has been calculated via the Kissinger plot found in Figure 2. This indicates a decrease of approximately 85 and 11 kJ/mol for Mg_2FeH_6 and MgH_2 , respectively [4, 5]. This decrease in E_a is a result of the addition of Fe into the material and a reduction in the particle size of the material. The unreacted Fe acts as a catalyst and results in a decrease in the energy required for H_2 desorption. In combination with the smaller particles, the decrease in the E_a leads to improved absorption/desorption kinetics and potentially faster charge/discharge rates for the material. The high temperature material, NaMgH_3 was also synthesized. NaMgH_3 was initially investigated as a high enthalpy heat storage material due to its favorable thermodynamic properties and low cost. This was achieved by a solid state synthesis route utilizing a combination of ball milling in addition to hydrogenation at elevated temperatures. X-Ray Diffraction (XRD) confirmed the presence of the desired NaMgH_3 phase.

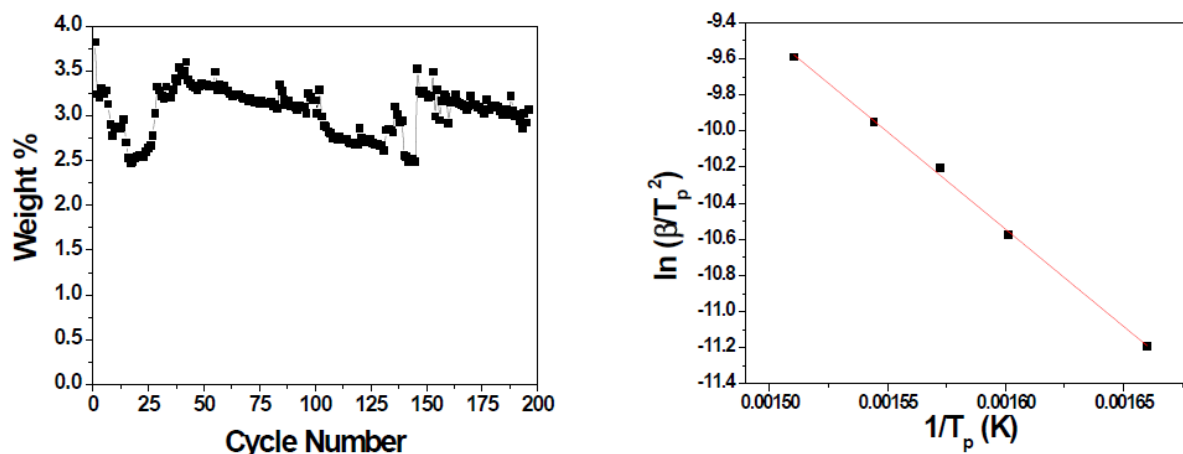


Figure 2: (left) Cycle stability of Mg_2FeH_6 at a pressure of 95 bar H_2 and 500°C and (right) Kissinger Plot for Mg_2FeH_6 (MgH_2 rich).

The material was synthesized with a slight excess of NaH to ensure a complete reaction and to minimize the segregation of material as was done previously with $NaAlH_4$ materials. The material was cycled 10 times and stopped to analyze the material by XRD and Thermal Gravimetric Analysis (TGA) to determine if the material retained its original composition. When the reactor was opened, the entire inside of the reactor was found to have been coated with a powder, indicating that the material had vaporized during the cycling experiment. It was found that $NaMgH_3$ segregates into separate materials at high temperatures with cycling due to the volatile nature of sodium which is a product of the decomposition. This leads to the formation of NaH and MgH_2 in separate regions of the reactor (i.e. the cooler region containing the NaH). In order to circumvent this limitation, the addition of F as $NaMgH_2F$ was investigated to increase the stability of the sodium product formed (NaF) and to achieve a higher enthalpy of reaction. The formation of $NaMgH_2F$ was monitored by XRD during its synthesis. This involved the ball-milling of NaF and magnesium in stoichiometric amounts followed by annealing under hydrogen pressure and elevated temperatures to form $NaMgH_2F$. The XRD of the material at various stages of the formation is shown in Figure 3. The black spectra represent the starting material and the green spectra the material after the synthesis process. The green spectra demonstrated that a very pure phase of $NaMgH_2F$ was obtained. A rietveld analysis of the synthesized $NaMgH_2F$ material revealed that it was the only crystalline product in the sample and was 94.31 wt. % of the sample with 5.69 wt. % of an amorphous component. The activation energy (Figure 4) for desorption of $NaMgH_2F$ was determined from the Kissinger plot of TGA data at differing temperature ramp rates. The measured activation energy for desorption was 151.5 ± 1.8 KJ/mol.

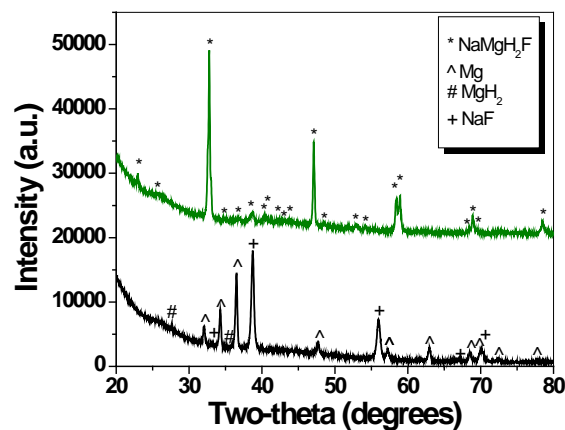


Figure 3: XRD of the synthesis of the high temperature NaMgH₂F material.

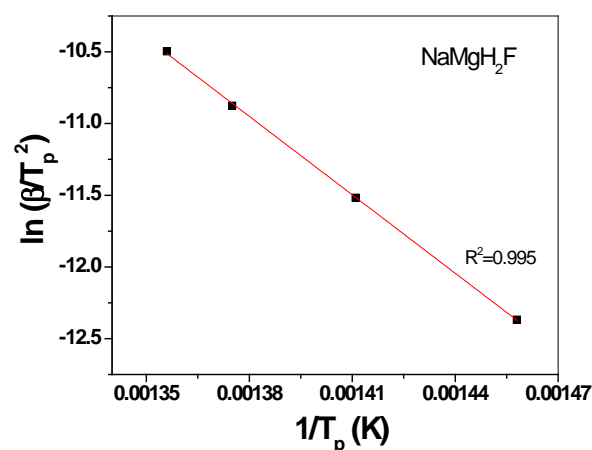


Figure 4: Kissinger plot obtained from TGA data for NaMgH₂F. (151.5 ± 1.8 kJ/mol)

Figure 5 shows the first 10 cycles of NaMgH₃ and NaMgH₂F at 500 °C. The material was cycled between 1 bar (desorption) and 45 bar (absorption) of hydrogen with cycle times of 3 hours. To our surprise, NaMgH₂F displayed a lower cycle stability than NaMgH₃. NaMgH₂F was determined to also lose capacity from loss of volatile Na. This suggests that the mechanism of the reaction proceeds through NaH or Na metal at some point instead of being bound to the fluorine at all times. Further modifications to this material may still be warranted to prevent the Na volatility and improve its cycling stability.

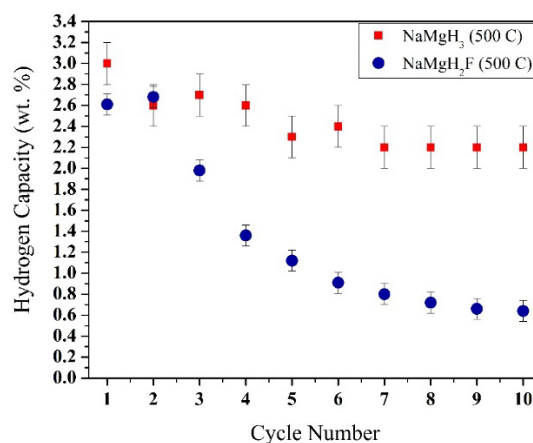


Figure 5: First 10 cycles of the high temperature NaMgH₃ material with hydrogenation at 600°C and 70 bar and dehydrogenation at 600°C and 1 bar H₂.

2.1.1.2 Low Temperature Material Evaluation and Performance

Extended cycling and modification to the low temperature metal hydride material, NaAlH₄ (SAH), was carried out. More than 1000 hydrogen absorption/desorption cycles on NaAlH₄ and modified NaAlH₄ materials were performed. The modifications to NaAlH₄ materials were all made to the original cycled material, as opposed to new materials, in an effort to create more stable and less kinetically hindered materials for continuous cycling. Through the incorporation of expanded natural graphite (ENG) into the NaAlH₄ (SAH) the material's thermal conductivity and stability were increased compared to that of previous modifications. More than 700 absorption/desorption cycles were performed with this modified material. Figure 6 (black) compares the results from the absorption/desorption cycling of this material at the same temperature and pressure used for the other modification to the SAH material. As shown, the SAH modified with ENG retained a high capacity over +500 cycles, after which a drop to just below 3 wt% was observed over a period of 150 cycles. A portion of this capacity loss was recovered via mixing with a mortar and pestle and through a melt infiltration process (described below). The average current capacity for the recovered SAH is approximately 3.2 wt. %, indicating that the material may gradually separate over multiple cycles. During the melt infiltration process, the SAH (in the hydrogenated state) is heated to 190°C under a pressure of 140 bar H₂. Under these conditions, the SAH melts but does not release its hydrogen content. During this process it was attempted to see if the SAH in the molten state would re-homogenize the material and recover capacity. However, this process was only moderately successful and it is believed that it might be more effective if this was performed earlier on in the cycling study and with more frequency.

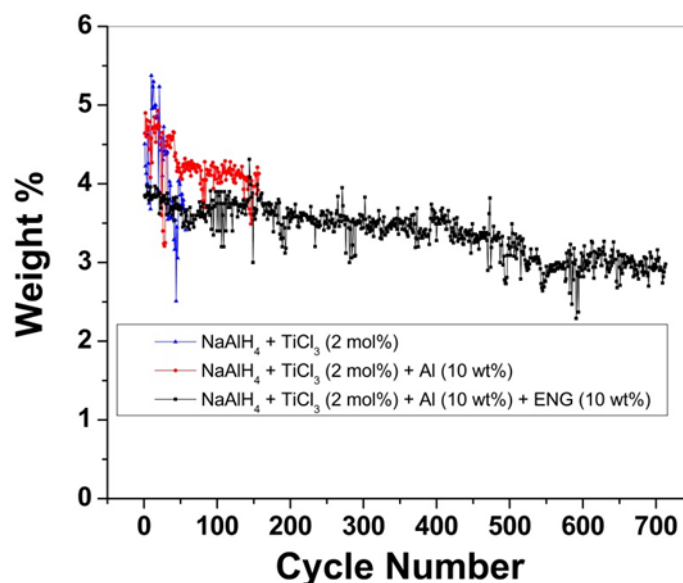


Figure 6: NaAlH₄-TiCl₃ (2 mol%) modifications and extended cycling data.

Figure 7 shows the Kissinger plot for the ENG modified SAH material. The results indicate a decrease in the activation energy for desorption compared to those of pure

SAH and SAH catalyzed with TiCl_3 . An activation energy of 70.6 ± 0.9 kJ/mol and 118.6 ± 1.2 kJ/mol for the 1st and 2nd desorption steps, respectively, was determined. Compared to pure SAH, this shows a decrease in the E_a of approximately 50 and 24 kJ/mol for the 1st and 2nd desorption steps, respectively. This also shows a slight (approximately 8-10 kJ/mol) decrease in the 1st desorption step when compared to the TiCl_3 catalyzed SAH.

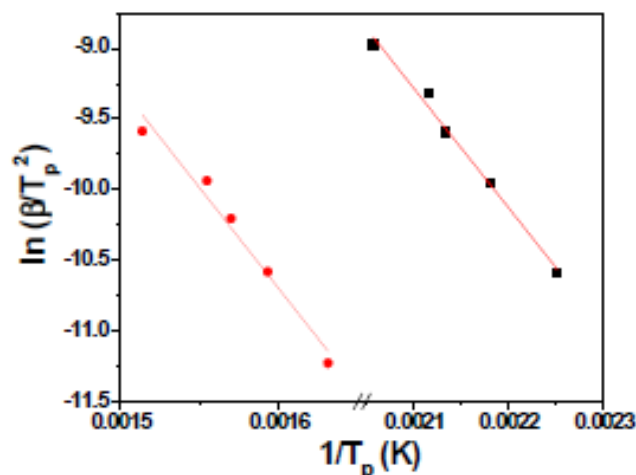


Figure 7: Kissinger Plot for the NaAlH_4 - TiCl_3 -Al-ENG. The 1st desorption step is shown using red circles and the 2nd step is shown in black squares.

To increase cycle stability and lower the operating pressures required for the low temperature metal hydride Na_3AlH_6 was considered [4]. The Na_3AlH_6 material was prepared by first ball milling a 2:1 ratio of NaH and NaAlH_4 , followed by doping with a Ti-based catalyst. The formation of the material was confirmed using XRD analysis. Initial studies [6] have shown that the material demonstrates very stable cycling capacity relative to SAH (NaAlH_4). This system also possesses several advantages over the NaAlH_4 -based material: 1) it is a simple one-step desorption process, 2) the pressure required for regeneration is lower (~ 8 bar H_2 at 150°C) than that of NaAlH_4 , which may prevent the segregation of materials in the system, leading to faster rate of re-hydrogenation with less capacity fade, and 3) it should exhibit improved kinetics. However, this material will also require a slightly higher operating temperature ($\sim 150^\circ\text{C}$) and has a lower capacity (3.0 wt. %). It is believed that the stability and pressure advantages of this material will outweigh the disadvantages of lower capacity and a temperature increase. Figure 8 shows the XRD of the synthesis of the Na_3AlH_6 utilizing the ball milling approach. The XRD shows that Na_3AlH_6 has been formed with some of the NaH starting material still present. This indicates that more NaAlH_4 needs to be added to the milling reaction in order to fully consume the NaH to form more of the Na_3AlH_6 . The excess NaAlH_4 used can then be washed away with ether since the Na_3AlH_6 is insoluble. The formation of NaCl is due to the metathesis reaction between NaAlH_4 and TiCl_3 indicating that the Ti doping of the material was successful.

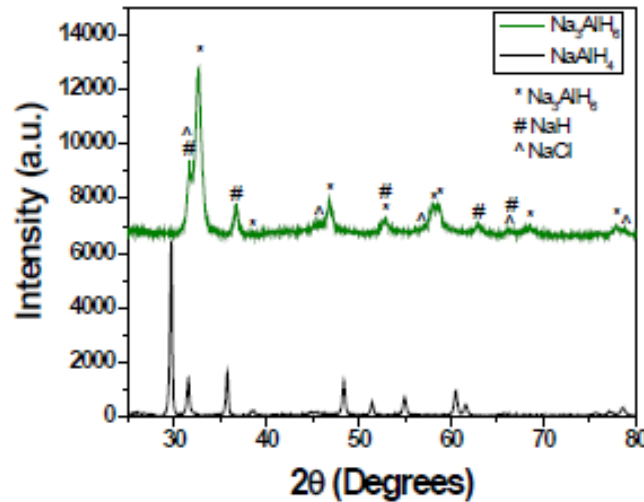


Figure 8: Ball-milling synthesis of Na_3AlH_6 from $\text{NaAlH}_4/\text{NaH}/\text{TiCl}_3$.

Cycling experiments (see Figure 9) were initiated utilizing the Na_3AlH_6 material prepared from this process to determine the optimum operating conditions for the material [7]. Operating temperatures between 150 and 160°C and pressures between 20 and 40 bar of H_2 were examined. This material was found to have an extremely stable cycling capacity in the 150 cycles performed thus far. This study indicated that the optimum operating conditions for extended cycling are 30 bar H_2 and 150°C. It was also observed that the re-hydrogenation of this material was faster relative to the parent NaAlH_4 material. As shown in Figure 10, the rate at which the Na_3AlH_6 absorbs hydrogen is slightly better than the parent NaAlH_4 material and is achieved at a much lower pressure as well (30 bar H_2 vs. 90 bar H_2).

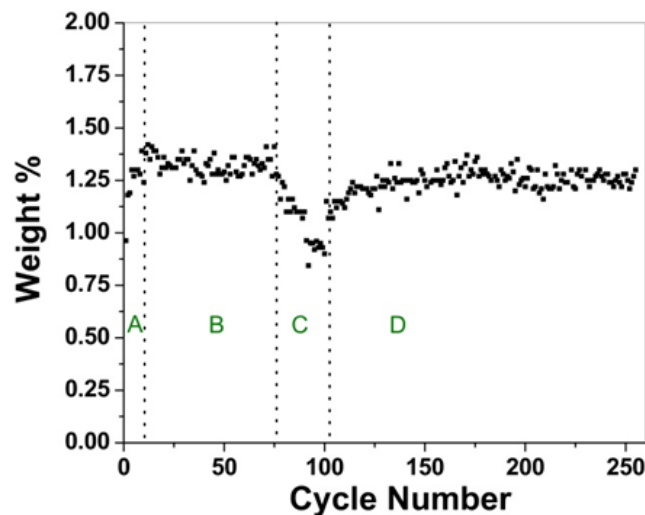


Figure 9: Cycling optimization of the low temperature Na_3AlH_6 material. Hydrogenation conditions are: (A) 20 bar H_2 , 150°C, (B) 40 bar H_2 , 160°C, (C) 20 bar H_2 , 160°C, (D) 30 bar H_2 , 150°C

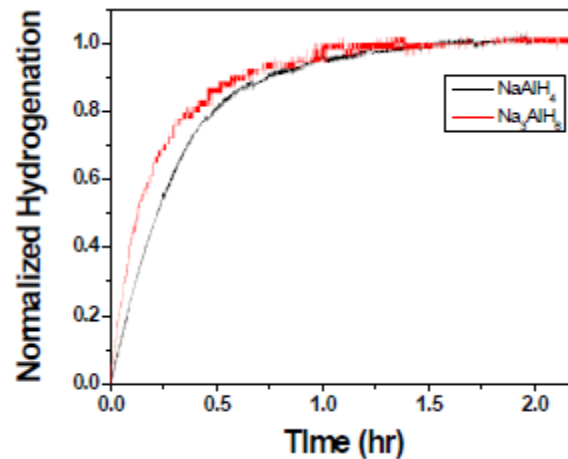


Figure 10: Comparison of the rate of hydrogenation of the NaAlH_4 and the Na_3AlH_6 LTMH candidates.

For comparison purposes the cycling stability of the NaAlH_4 and Na_3AlH_6 materials when both were cycled at 130°C are shown in Figure 11. The Na_3AlH_6 is cycled at a pressure of 30 bar H_2 while the NaAlH_4 is cycled at a much higher 100 bar of H_2 . The capacity of the Na_3AlH_6 is more stable than the NaAlH_4 for the cycles measured.

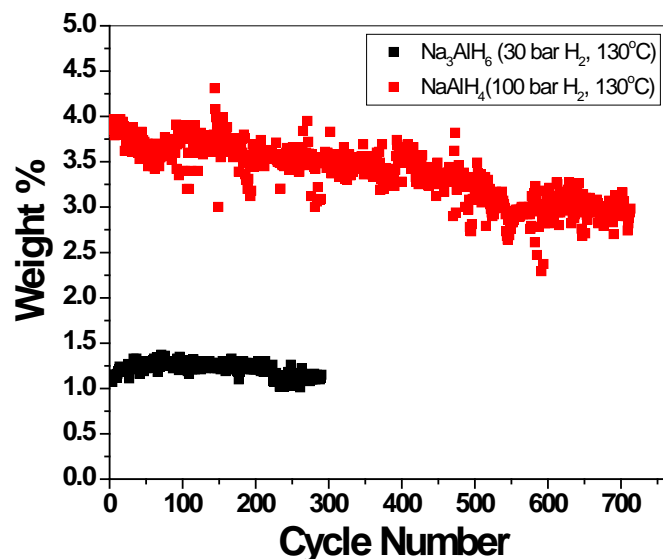


Figure 11: Comparison of cycle stability of the NaAlH_4 and Na_3AlH_6 materials.

2.1.2 Modify and Engineer MH Materials to Meet SunShot Targets

In order to reach Sunshot targets, promising material candidates were modified to alter their thermodynamic and kinetic properties. This was carried out in the case of CaH_2 by the addition of Al and Si to form reversible alloys. These alloys allow for the capture of highly corrosive molten CaH_2 and increase the equilibrium pressure to a more useful value for the hydrogenation of the low temperature metal hydride (LTMH). For the LTMH, thermal conduction additives and a catalyst was added to promote reversibility, enhance hydrogen capacity, and increase thermal conductivity.

2.1.2.1 High Temperature Material Synthesis and Material Evaluation

In order to stabilize CaH₂ and modify the thermodynamic properties, aluminum was added. The alloys CaAl₂ and CaAl were found to be viable candidates for the high temperature metal hydride at temperatures below 650 °C. The reaction in the CaAl₂ proceeds as follows:

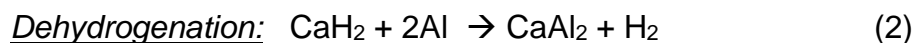
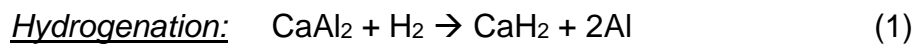


Figure 12 below demonstrates a 1.8 wt. % capacity for the hydrogenated CaAl₂ alloy after cycling at 650 °C and 95 bar H₂ for 6 hour cycles. Reversibility of the CaAl₂ and crystal phase identification was accomplished using powder XRD. Figure 13 displays diffraction patterns for the hydrogenated and dehydrogenated CaAl₂ material. In the hydrogenated state, CaH₂ and Al are present and in the dehydrogenated state only CaAl₂ is present.

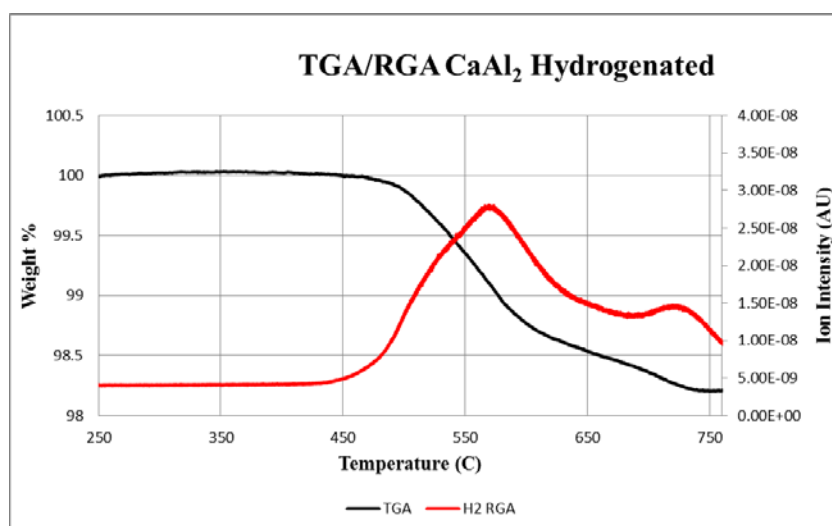


Figure 12: TGA/RGA of CaAl₂ hydrogenated at 650 °C and 95 bar H₂ for 6 hours.

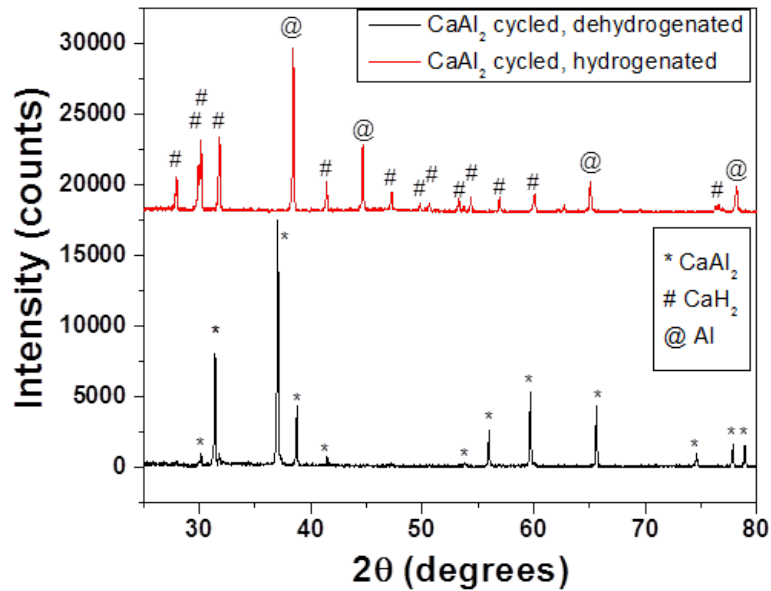


Figure 13: XRD spectra of CaAl₂ hydrogenated for 6 hours at 95 bar H₂ and 650 °C (red) and the dehydrogenated material (black).

A new method was also developed for stabilizing the NaMgH₂F material at temperature above 650 °C by the incorporation of ½ mole Si. This allows for the stabilization of the Mg metal which has a significant vapor pressure above 600 °C. Data for this material is shown in Figure 15 below. The incorporation of Si to NaMgH₂F led to the formation of Mg₂Si which allows for higher temperature operation assuming the Na can be stabilized as well.

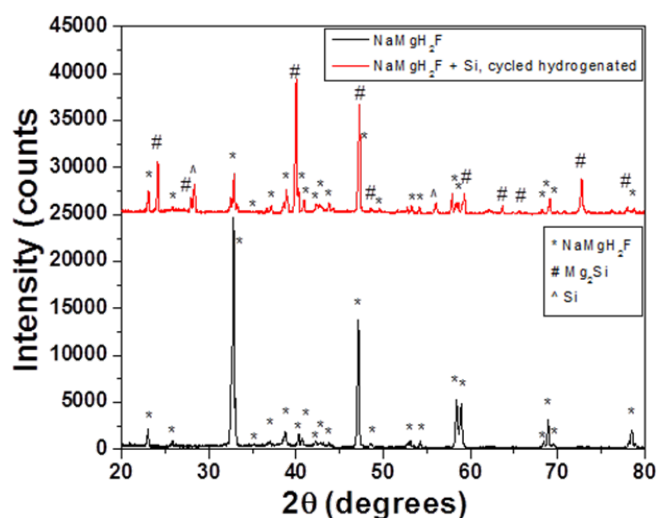


Figure 15: XRD spectrum showing the stabilization of Mg with Si after incorporation into NaMgH₂F.

To operate at temperatures above 650 °C materials based on Ca and Si were developed. The Ca₂Si material was cycled 117 times at 750 °C with a desorption pressure of 2.5 bar and an absorption pressure of 49 bar over 3 hour cycles.

Hydrogen capacities were determined by Thermal Gravimetric Analysis (TGA). The cycling was stopped and hydrogen capacities were measured at 21 cycles, 42 cycles, and 71 cycles and are shown in Figure 16. TGA measurements show a stable hydrogen capacity of ~1.8 wt. % over the 71 cycles.

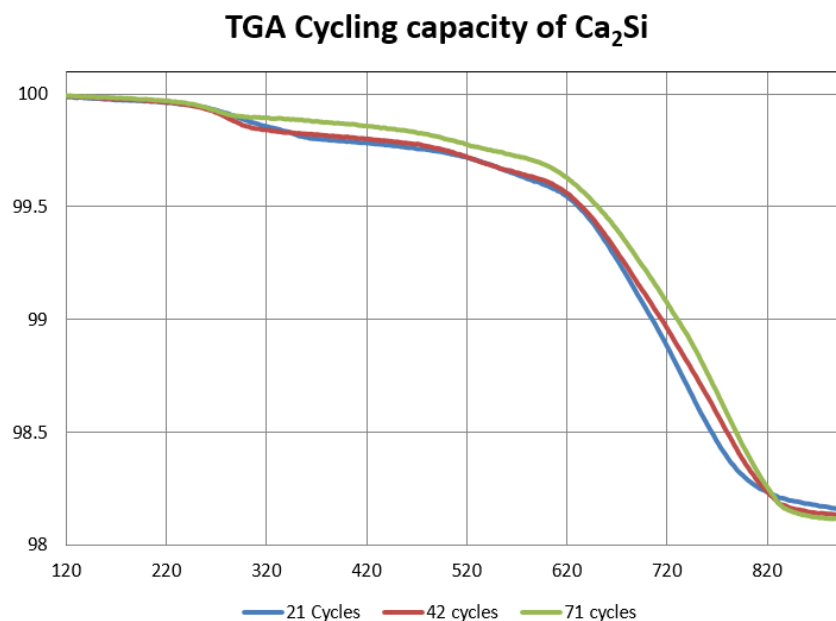


Figure 16: TGA data of Ca₂Si after various cycle numbers cycled at 750 C and 49 bar for 3 hour cycles.

Thermal conductivity measurements of the Ca₂Si material were carried out at the University of Pavia. The results and extrapolation are shown in Figure 17. At 700 °C the thermal conductivity is expected to be ~0.4 W/mK, which is comparable to many other metal hydrides. This thermal conductivity can be increased with the addition of additives (copper, expanded natural graphite, etc.) as was shown previously with SAH. The density of the dehydrogenated material was determined to be 0.8 g/ mL for the loose powder and ~ 4 g/mL for a pellet compressed at 4 tons. Further investigation into enhancing this material (with the addition of additives) and understanding the mechanisms of dehydrogenation and re-hydrogenation will be carried out under a current SRNL funded LDRD project.

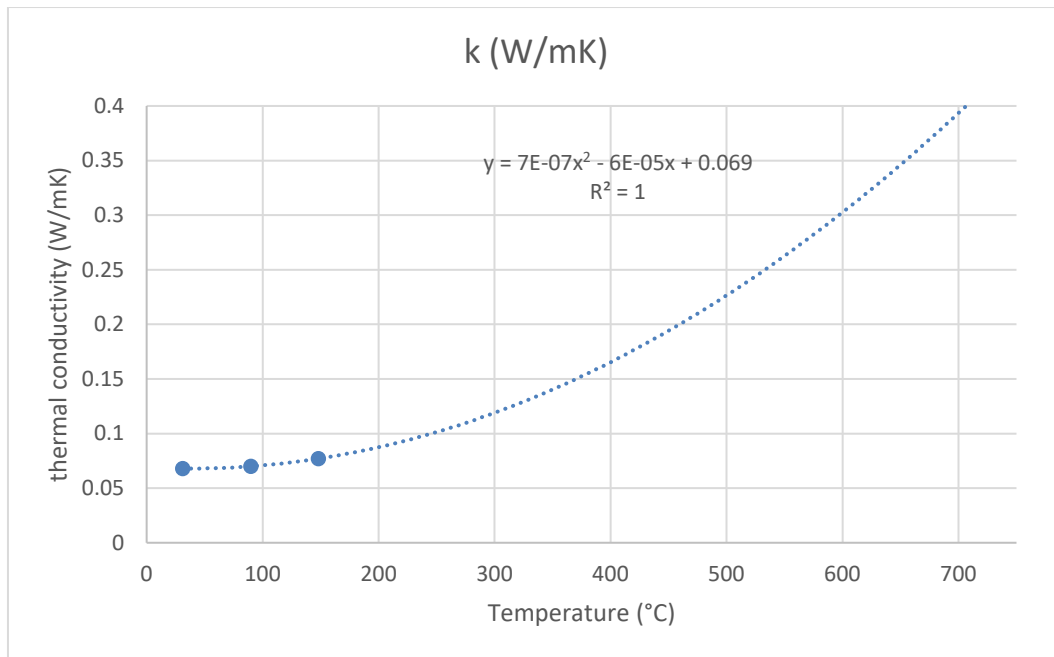


Figure 17: Thermal conductivity of Ca_2Si material after cycling. (Hydrogenated)

The activation energy for the dehydrogenation of CaH_2 and Si in a 2:1 ratio was determined by the Kissinger method using TGA as shown in Figure 18. The activation energy was determined to be 142 ± 10.7 kJ/mol.

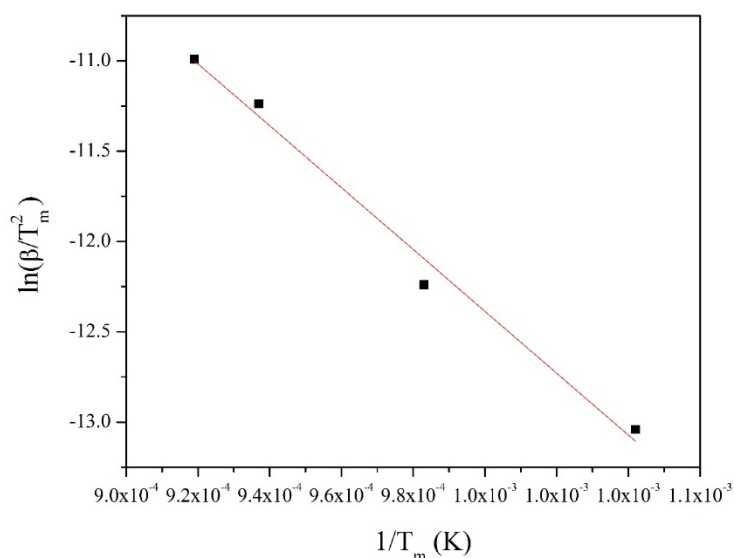


Figure 18: Kissinger Plot of CaH_2 :Si (2:1 molar ratio) acquired from TGA data at various ramp rates

2.1.2.1 Low Temperature Material Evaluation and Performance

Na_3AlH_6 was chosen as the low temperature metal hydride material due to its cycle stability. Na_3AlH_6 was cycled without the use of additives and the material was found

to be stable for over 200 cycles. It was recently discovered that the addition of ENG and Al to this material increases the accessible capacity of the material as shown below in figure 20. This effect is likely due to an increase in the thermal conductivity of the material from the additives. The incorporation of these additives lowers the cost by decreasing the amount of material required for the thermal energy storage system. There is no observable degradation over 140 cycles in the modified Na_3AlH_6 material as shown below. The slight increase is due to the system reaching an optimized particle size and atomic proximity after many absorption/desorption cycles.

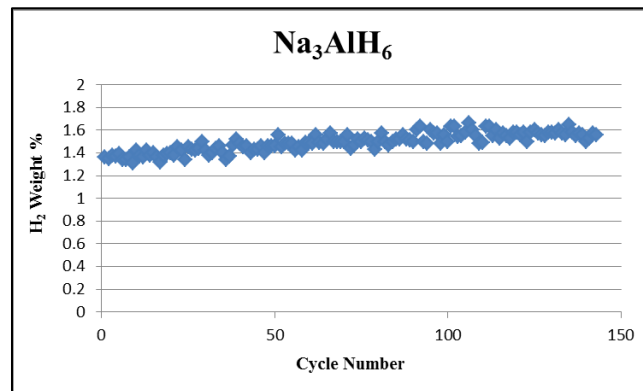


Figure 19: Cycling data for modified low temperature material ($\text{Na}_3\text{AlH}_6 + \text{TiCl}_3 + \text{ENG} + \text{Al}$). (Note: The weight percent shown is the total capacity of the composite.)

2.2. Screening Tool, Cost and Performance Model Development and Application

2.2.1 Development and evaluation of screening tools

A screening tool has been set up during Period 1 of the project, including: (1) the cost of the overall TES system (i.e. including MH material cost, heat exchanger cost and pressure vessel cost), (2) the exergetic efficiency of the TES system integrated with the solar receiver and the power plant, (3) the volumetric efficiency of the TES system. Details on the models adopted to evaluate the cost and the exergy of the system can be found in the previous reports and in the publications from the current project [3, 8]. While all the MH based TES systems met and exceeded the DOE volumetric efficiency (all the MH systems showed values at least on the order of 100 kWh/m^3), the most aggressive targets to be achieved were represented by the cost and the exergetic efficiency of the TES system.

Modify MH materials to meet DOE SunShot Targets – During Period 1, SRNL and CU collected and evaluated material property data for more than 20 MH candidates [3]. From these materials three potential pairs of materials were selected as the most promising existing materials capable of meeting many of the DOE SunShot targets. These material pairs included:

$\text{Mg}_2\text{Fe}_3\text{H}_6/\text{NaMgH}_3$ – SAH (Sodium Aluminum Hydride)
 $\text{TiH}_{1.72}$ – TiXY (where X & Y are typically Fe, Mn)
 CaH_2 – TiXY.

Results for the specific cost and exergetic efficiency of the three down selected MH pairs are shown in Figures 20 and 21.

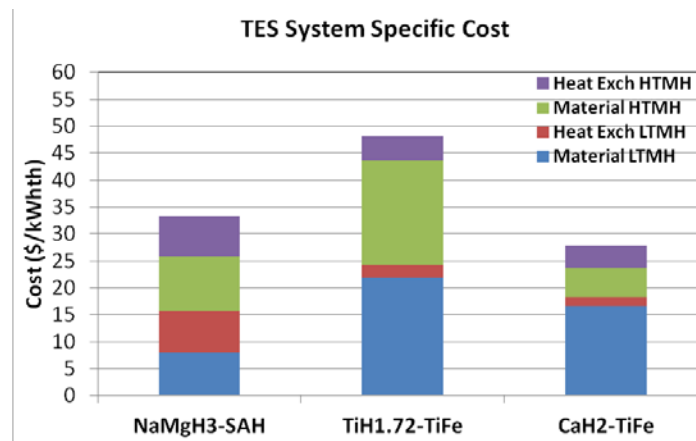


Figure 20: Specific cost (\$/kWhth) of the three pairs down selected during Period 1.

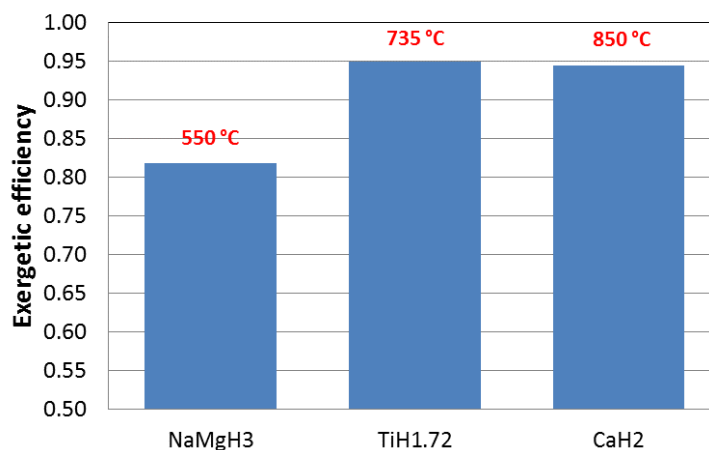


Figure 21: Exergetic efficiency of the three pairs down selected during Period 1.

In addition to the results shown above, the third pair ($\text{CaH}_2\text{-TiFeH}_2$) is known to have corrosion issues related to the melting and evaporation of the Ca hydride. This has to be overcome before making the pair an actual feasible TES system for large scale applications. Therefore, the major objective of Period 2 was to modify these materials to enhance their system performance to meet all the targets.

As described previously in Section 2.1, SRNL and CU concentrated on 3 main material modifications for the high temperature metal hydride (HTMH) materials. A fluoride modified sodium magnesium material (NaMgH_2F) that not only lowers cost and raises operating temperatures but also minimizes the evaporation and deposition of Mg that was found to occur at higher temperatures. The other two modifications involved changes to the higher temperature Ti and Ca materials. Modification to the Ti system examined alloying Ti with Al to help lower the cost of the material. Recent attempts to modify CaH_2 , which is a very high temperature and a very low cost hydride material, resulted in the development of a new patent by SRNL [1]. A new class of Ca based materials was identified as high potential HTMH

materials. Depending on the operating conditions and properties, Ca can be linked with either Al or Si at different ratios. Among the examined materials, CaAl and Ca₂Si were identified as potential high performance materials, being able to reach temperatures of 650 °C or higher and to reduce the overall TES system cost. The new Ca based system has shown the potential to create a HTMH material that is not only low cost and high temperature but also mitigates unwanted material melting and evaporation. For the LTMH material pairing the hexa-hydride form of SAH (Na₃AlH₆) was identified and evaluated as an improved alternative to SAH that operates at lower pressure and has better cycling stability.

The main objective during Period 2 and (partially) Period 3 was the performance evaluation of modified MH materials, comparing them with 'ideal' MH materials. The performance of two modified materials (NaMgH₂F and TiAlH_x) was evaluated during Period 2. The last results are included in the report, along with some of the analyses carried out for the new material¹ developed at SRNL.

Modified materials

High pressure system (NaMg based HTMH – SAH LTMH)

The first modified material, to be used in a high pressure system, is based on the Mg family and consists of the inclusion of F in the NaMg material resulting in the compound NaMgH₂F. The properties of the modified material, needed to evaluate the steady state techno-economic system performance, are reported in Table 2, based on Reference [8].

Table 2: NaMgH₂F material properties [8]

	NaMgH ₂ F	SAH
Reaction enthalpy ΔH (kJ/molH ₂)	96.8	40
Reaction entropy ΔS (J/molH ₂ K)	134	130
Bulk density (kg/m ³)	1390	750
Weight capacity (kgH ₂ /kgmatl)	0.029	0.037
Cost of raw material (\$/kg)	1.73	3
Typical operating temperature (°C) /pressure (bar)	650/50	100-120/50-70

Compared to the unmodified material (NaMgH₃), the F modified material shows a higher reaction enthalpy, corresponding to higher operating temperature (keeping approximately the same operating pressures). This results in a reduction of the total amount of hydrogen to be stored and, consequently, a reduction in the mass of hydrides (i.e. lower cost). In addition, the cost of the raw material shows a reduction of about 58% compared to the NaMgH₃ material cost, due to the fact that the NaF compound (mixed with Mg to make the final material) is an inexpensive material. This material can be paired with SAH (given the high operating pressure around 40 bar), making the pair less expensive than the unmodified material (NaMgH₃) system.

Medium pressure system (Ca₂Si based HTMH – Na₃AlH₆ LTMH)

¹ Most of the results reported in the current document refer to Ca₂Si material.

The second modified material, to be used in a pressure system with working pressures on the order of 10-30 bar, is based on a new material (Ca_2Si) developed at SRNL. The (preliminary) properties² assumed for the modified material, needed to evaluate the steady state techno-economic system performance, are reported in Table 3, along with the properties of the hexahydride (Na_3AlH_6) material. A ΔT of 30 °C has also been assumed to design the heat exchangers, since the HTMH material can achieve (based on its properties) good exergetic efficiencies at temperatures of 650-700 °C (as also reported in the following figures). More details on the hexahydride material properties can be found in previous reports [9].

Table 3: Ca_2Si - Na_3AlH_6 material properties

	Ca_2Si	Na_3AlH_6
Reaction enthalpy ΔH (kJ/molH ₂)	105	47
Reaction entropy ΔS (J/molH ₂ K)	131	134
Bulk density (kg/m ³)	1200	750
Weight capacity (kgH ₂ /kgmatl)	0.035	0.025
Cost of raw material (\$/kg)	1.6	3
Typical operating temperature (°C) /pressure (bar)	650-700/15-20	120/10-20

Low pressure system (Ti based HTMH – Na_3AlH_6 LTMH)

The third modified material, to be evaluated at a lower working pressure (on the order of 5-10 bar) system, is based on the Ti HTMH family and contains the inclusion of Al in the HTMH compound. The following main techno-economic drawbacks for the TiH_2 HTMH were identified during the project: 1) the HTMH material (TiH_2) raw cost was too high to achieve the final economic target; 2) the low operating pressure of the HTMH material made it possible to pair it only with a Ti-based LTMH material (i.e. expensive MH). The techno-economic analysis carried out for the low pressure system modified MH is only preliminary and it is based on preliminary evaluations carried out at SRNL and on data reported in the literature [10]. Based on the data available, the compound Ti_3AlH_x is expected to form (with $x=5-8$) [10]. The baseline (assumed) value so far is $x=7$, giving a weight capacity on the order of 4.1%, on the basis of data reported in literature [11].

The properties of the TiAlH_x material, needed to evaluate the steady state techno-economic performance, are reported in Table 4.

Table 4: TiAlH_x material (HTMH) properties

Reaction enthalpy ΔH (kJ/molH ₂)	120	Assumed based on the TiH_2 reaction enthalpy and increase of pressure up to around 5-10 bar
Reaction entropy ΔS (J/molH ₂ K)	130	Assumed based on the TiH_2 reaction entropy and considering the HTMH material values are on the order of 130 J/mol K (see below as well)
Bulk density (kg/m ³)	1500	Based on Ti and Al density
Weight capacity (kgH ₂ /kgmatl)	0.04	Reference [10]
Cost of raw material (\$/kg)	8	Based on Ti and Al cost
Typical operating temperature (°C) /pressure (bar)	720/10-15	Assumed based on inclusion of Al in the TiH_2 material, resulting in lowering T and increasing P

² Additional experimental activities are being carried out to verify the preliminary thermodynamic properties, reported in the table, (especially: ΔH and weight capacity) and get more accurate data.

The main HTMH properties to be highlighted are the decrease of the raw material cost and, above all, the increase of the operating pressure which opens new solutions to pair the material with a less expensive LTMH, such as Na_3AlH_6 . The properties of Na_3AlH_6 are reported in Table 2.

Modified materials techno-economic analysis results

Adopting the methodology described in Reference [3], the results of the techno-economic analysis carried out for the three new developed materials are reported in Figures 22 and 23. The most promising materials are NaMgH_2F and the Ca_2Si material, which show an installed cost on the order of 25 \$/kWhth and exergetic efficiency values very close to the final SunShot target.

It is important to highlight that: (1) no additional LTMH material modifications have been examined (the SAH based materials have been selected as the baseline materials); (2) no heat transfer system optimization has been performed.

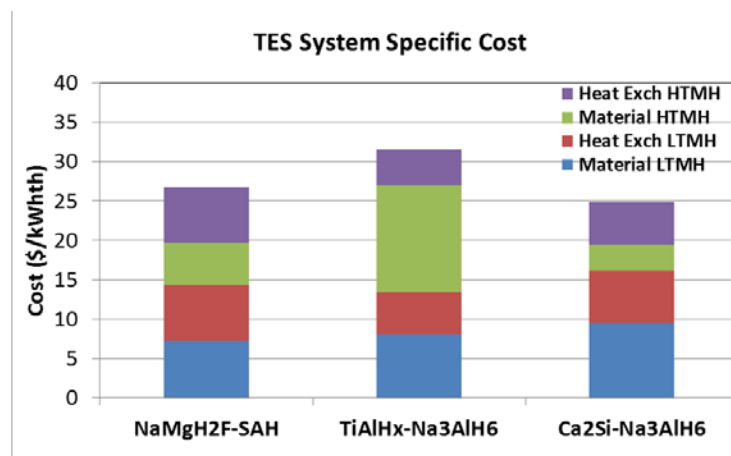


Figure 22: HTMH modified material system installed specific cost

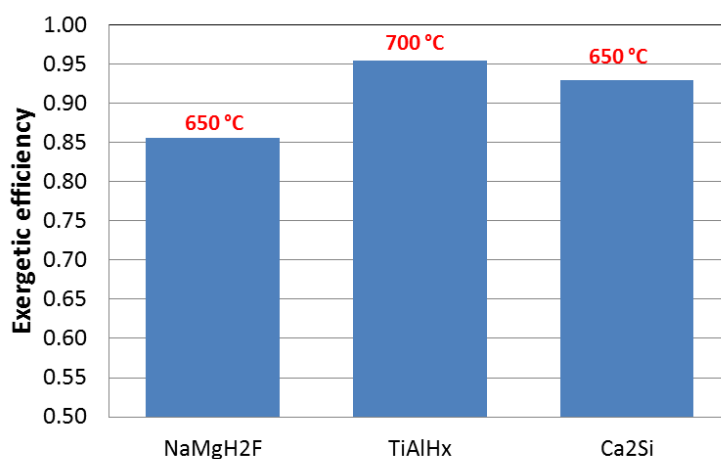


Figure 23: HTMH modified material exergetic efficiency

The Ca based material showed the best potential to approach and meet the DOE targets. During Period 2, sensitivity analyses were carried out looking at the cost variation of the selected system by varying: (1) HTMH weight capacity (the worst

case scenario is based on a reduction of 10%), (2) LTMH weight capacity (the worst case scenario is based on a reduction of 15%), (3) thermal conductivity (the worst case scenario is based on a reduction of the thermal conductivity of 20%). Results are reported in Figure 24 with the worst case scenario identified as 'WSCa2Si-Na3AlH6' and the baseline case identified as 'Ca2Si-Na3AlH6'.

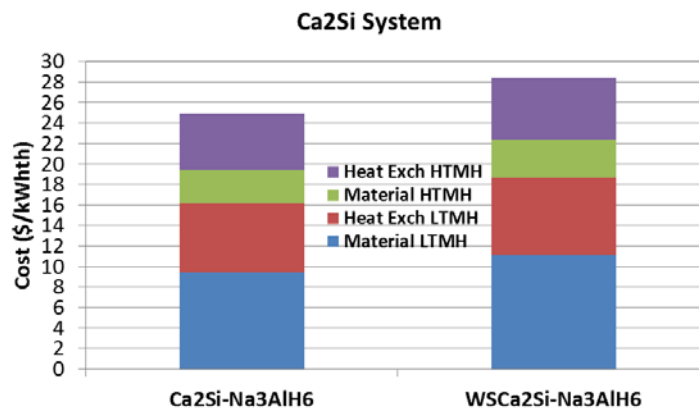


Figure 24: Variation of the specific cost of the TES system, varying the HTMH wf of 10%, LTMH wf of 15% and MH thermal conductivity of 20%

Ideal MH material properties

Based on the results obtained for the modified materials, the ideal material properties (for both the high pressure and lower pressure systems) have been assessed. The objective of this study was to determine what properties an ideal material would need to have to be able to achieve the DOE targets. Such properties have been compared with the properties available from experimental tests carried out on the new modified materials, adopting the probabilistic approach discussed in the next sections.

The current HTMH properties have been collected to form a database. Physical and chemical properties of the ideal materials have been assumed based on the data available for HTMH. Additionally, assumptions regarding the techno-economic properties of the ideal material were made with the objective of attaining system costs and exergetic efficiencies close to the targets. Following the approach highlighted previously, two systems have been considered. One is a high pressure ideal system which contains the ideal HTMH material (referred to as IdHTMH1) coupled with SAH* material (the LTMH material has been assumed to have approximately the same properties as the SAH material). The lower pressure ideal system contains the ideal HTMH material (referred to as IdHTMH2) coupled with Na₃AlH₆* material (the LTMH material has been assumed to have approximately the same properties as the Na₃AlH₆ material). The properties of the IdHTMH1-SAH* system are reported in Table 5 and are compared with those of the NaMgH₂F-SAH system.

Table 5: Ideal system (IdHTMH1-SAH*) and NaMgH₂F-SAH properties

	IdHTMH1	NaMgH ₂ F	SAH*	SAH
ΔH (kJ/molH ₂)	98	96.8	40	40
ΔS (J/molH ₂)	131	134	125	125
ρ (kg/m ³)	1600	1390	900	750

wf	0.04	0.029	0.04	0.037
Raw matl cost (\$/kg)	1.75	1.73	2.8	3
Operating P range (bar)	30-40	40	30-40	40
k (W/mK)	7	7	7	7
ΔT (K)	40	25	40	25
h_{conv} (W/m ² K)	2000	2000	2000	2000

The properties of the IdHTMH2- Na₃AlH₆* system are reported in Table 6 and compared with those of the Ca₂Si- Na₃AlH₆ system.

Table 6: Ideal system (IdHTMH2- Na₃AlH₆*) and Ca₂Si- Na₃AlH₆ properties

	IdHTMH2	Ca ₂ Si	Na₃AlH₆*	Na ₃ AlH ₆
ΔH (kJ/molH ₂)	110	105	45	47
ΔS (J/molH ₂)	130	131	134	134
ρ (kg/m ³)	1600	1200	900	750
wf	0.039	0.035	0.03	0.025
Raw matl cost (\$/kg)	1.75	1.6	2.8	3
Operating P range (bar)	10	15-20	10	15-20
k (W/mK)	7	7	7	7
ΔT (K)	40	30	40	30
h_{conv} (W/m ² K)	2000	2000	2000	2000

The specific costs of the ideal HTMH material-based systems are reported in Figure 25. The ideal HTMH materials are paired with the existing LTMH materials. The SAH* system cost represents about 55% of the IdHTMH1-SAH* cost, while the Na₃AlH₆* system cost represents almost 61% of the IdHTMH2-Na₃AlH₆* cost.

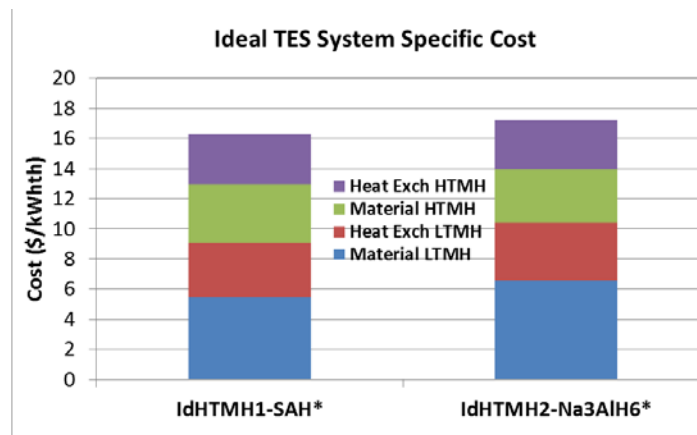


Figure 25: Ideal TES system specific cost for the high pressure (IdHTMH1-SAH*) and lower pressure (IdHTMH2-Na₃AlH₆*) systems

The exergetic efficiency of the two ideal HTMH material TES systems is reported in Figure 26. According to the evaluations and assumptions made above, the IdHTMH2 material, which has higher reaction enthalpy and lower pressure, works at a higher temperature compared to the IdHTMH1 material. Thus its exergetic efficiency (about 93%) is slightly higher than that of IdHTMH1 (about 86%)³.

³ The ΔT in the heat exchanger is equal to 40 °C. This reduces the cost of the system but also decreases the exergetic efficiency

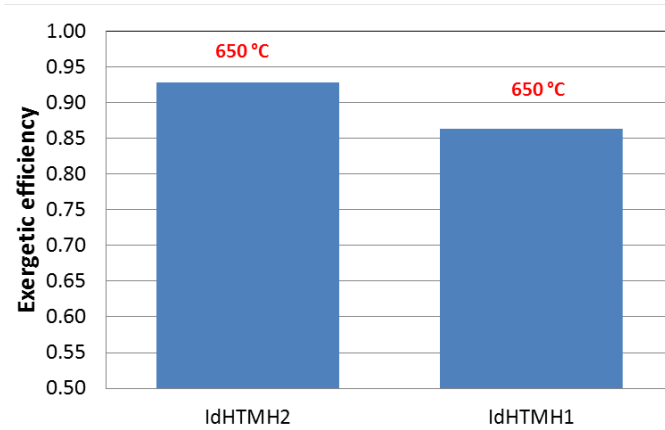


Figure 26: Exergetic efficiency of the two ideal MH systems

Statistical performance comparison with Ideal Materials

A performance comparison between the new developed materials and the ideal MH materials has been carried out at SRNL with the results shown below. The adopted general methodology is quickly described in this current document.

Methodology

The final formulation of the statistical approach is reported here as follows.

$$\mathfrak{S} = \sum_n |\epsilon_n| \Gamma_n \quad (3)$$

Equation 3 represents the metric for required improvement of the system, with Γ being the weighting factors (with the sum equal to 1) for the different objective functions and ϵ given by Equation 4, below.

$$\epsilon_n = \sqrt{\sum_i \left[\left(\frac{\partial \phi_n}{\partial \xi_i} \Big|_{\xi_{j \neq i}} \right)^2 \sigma_{\xi_i}^2 \right] + \sum_j \sum_k \left[\frac{\partial \phi_n}{\partial \xi_j} \Big|_{\xi_{l \neq j}} \frac{\partial \phi_n}{\partial \xi_k} \Big|_{\xi_{l \neq k}} cov(\xi_j, \xi_k) \right]} \quad (4)$$

The most challenging targets are the cost of the system ($n=1$) and the exergetic efficiency of the system ($n=2$). Among these targets, the most aggressive one is the economic target. Thus the cost weighting factor (Γ_1) has been assumed equal to 0.9, while the efficiency weighting factor (Γ_2) has been assumed equal to 0.1⁴. The analysis has been carried out with the aim of evaluating the performance ‘distance’ between the ideal MH material and the actual modified MH materials. Thus the degrees of freedom of the problem are those related to the material properties, assuming the actual heat transfer system and pressure vessel system are the same for the actual materials and the ideal materials. As a consequence, based on the analyses carried out for previous systems, the variance values ($\sigma_{\xi_i}^2$) (shown in Table 7) have been assumed based on the actual materials and the ideal materials properties reported in Table 4 and 5.

⁴ The values have been assumed after internal discussion at SRNL, based on a conservative point of view. They can be varied after further discussion with DOE or other institutions.

Table 7: Degrees of freedom and variance values for the two selected systems

ξ	σ_{ξ} NaMgH ₂ F- IdHTMH1	σ_{ξ} Ca ₂ Si- IdHTMH2	Comment
ΔH HTMH (kJ/mol)	1.2	5	Data based on Table 4 and 5. As reported in the previous documents, the Mg based material data have been obtained in conjunction with Curtin University (personal communications). The Ca based material data have been obtained from experiments and evaluations at SRNL
ΔS HTMH (kJ/mol K)	3	1	
ρ HTMH (kg/m ³)	210	400	
wf HTMH (%)	1.1	0.4	
Matl Price HTMH (\$/kg)	0.02	-0.15	
ΔH LTMH (kJ/mol)	0	2	
ρ LTMH (kg/m ³)	150	150	
wf LTMH (%)	0.3	0.4	
Matl Price LTMH (\$/kg)	0.2	0.2	
Operating P (bar)	10	5	

The values of ε and the improvement metric are reported in the following table. The value of the improvement metric is lower than 10% meeting the required project target.

Table 8: Improvement metric for the two selected systems

ε	NaMgH ₂ F	Ca ₂ Si
ε_1 (cost)	11%	9.5%
ε_2 (exergetic efficiency)	0.9%	2.7%
$\tilde{\varepsilon}$	<u>9.8%</u>	<u>8.9%</u>

Probabilistic economic analysis of the modified materials

In addition to the previous techno-economic assessment, additional economic analyses have been carried out to compare the actual system installed cost (based on the newly developed modified materials) to the economic target. The objective is to see if the new materials have potential to achieve the cost targets..

The values of the variance (2σ) for all the relevant degrees of freedom, quantities and properties have been assessed based on the available experimental data for the new materials (Curtin University and SRNL for the NaMgH₂F material and SRNL for the Ca₂Si material). Where some data are lacking, reasonable assumptions have been made, based upon the data available and the material properties [12]. A Gaussian distribution has been assumed for the relevant properties with the mean value and the 2σ value reported in Table 9.

Table 9: Mean and 2σ values for the main relevant material and system properties

	Mean value NaMgH ₂ F	2σ NaMgH ₂ F	Mean value Ca ₂ Si	2σ Ca ₂ Si
Matl Price HTMH (\$/kg)	1.73	1.65	1.6	1.1
Matl Price LTMH (\$/kg)	3	2.55	3	2.55
ΔH HTMH (kJ/mol)	96.8	100	105	108

ρ HTMH (kg/m ³)	1390	1620	1200	1600
ρ LTMH (kg/m ³)	750	1300	750	1300
Conv.coeff h HTMH (W/m ² K)	2000	4000	2000	4000
Conv.coeff h LTMH (W/m ² K)	2000	10000	2000	10000
k HTMH (W/mK)	7	8.5	7	8.5
k LTMH (W/mK)	7	8.5	7	8.5
Press Vessel Material HTMH	SS	SS347H	SS	SS347H
Press Vessel Material LTMH	SS	Al	SS	Al

The best case scenario is with the Ca based HTMH material and with the 2σ values of all the degrees of freedom and quantities reported in Table 9, resulting in a system cost of about 16 \$/kWhth.

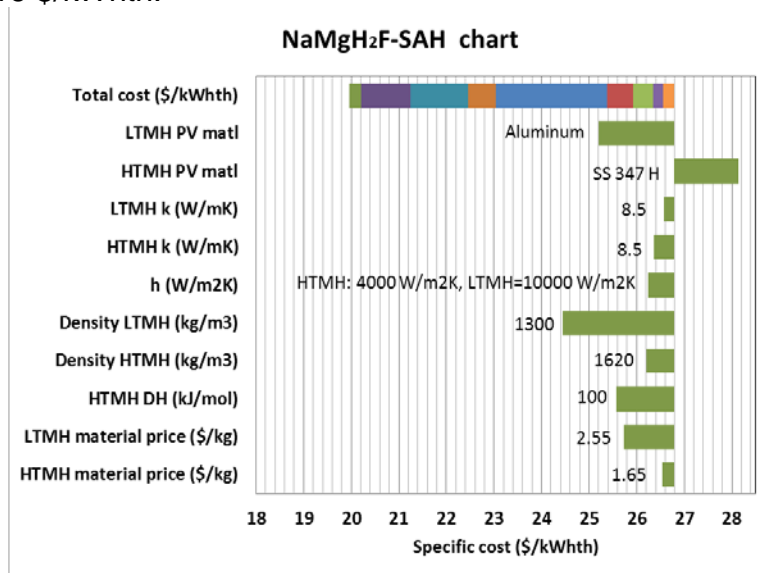


Figure 27: Probabilistic cost estimation for the Mg based system (the system cost is about 20 \$/kWhth). The influence of the 2σ values of the quantities on the cost is shown in the figure, with the first item ('Total cost') showing the total system cost variation (i.e. equal to the sum of the contributions shown as green colored bar charts).

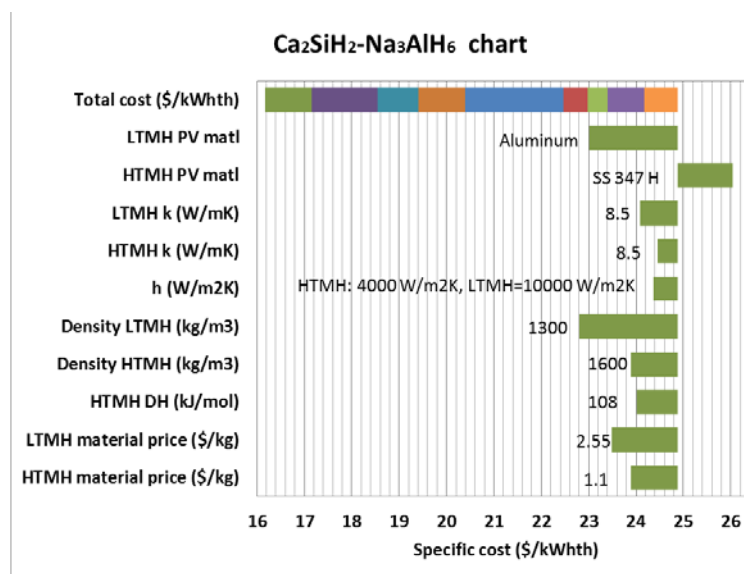


Figure 28: Probabilistic cost estimation for the Ca based system (the system cost reaches about 16 \$/kWhth). The influence of the 2σ values of the quantities on the cost is shown in the figure, with the first item ('Total cost') showing the total system cost variation (i.e. equal to the sum of the contributions shown as green colored bar charts).

2.2.2 Development and Evaluation of Transport and System MH TES Models

Numerical models both for detailed simulations (transport models) and system level analyses (system models) have been developed and selected simulations have been carried out. Detailed numerical transport models were used to examine the thermochemical behavior of two selected MH pairs (Mg_2FeH_6 - TiFeH_2 and NaMgH_2F - Na_3AlH_6). The first MH couple has been chosen based on the availability of the kinetics and thermodynamic data. The materials are known materials with available data from the literature and from experiments carried out at SRNL. However, the pair does not represent the final MH pair and does not meet all of the SunShot targets. The second material represents one of the most promising modified materials with potential of closely approach the targets. In addition, a MH system model has been developed in Matlab[®] and integrated into the overall CSP system model developed in TRNSYS[®]. The aim is to evaluate the behavior of the TES system interfaced with all the CSP plant equipment, highlighting the cycling ability and the potential to meet selected SunShot targets (such as the operating temperature). The current CSP plant model includes a steam power plant and a solar tower based concentration system along with the TES system.

Detailed Transport MH Models

The detailed transport model for the metal hydride bed simulation has been developed. The models are comprised of mass, momentum and energy balance equations with additional ancillary equations to evaluate the state and properties of hydrogen and kinetics expressions.

The adopted kinetics expression has the following form:

$$\frac{dX}{dt} = \begin{cases} C_a * \exp\left(\frac{-E_a}{RT}\right) * \ln\left(\frac{P}{P_{eq}}\right) * (X_M - X), & P > P_{eq}; \text{charging} \\ C_d * \exp\left(\frac{-E_d}{RT}\right) * \left(\frac{P - P_{eq}}{P_{eq}}\right) * (X - X_m), & P < P_{eq}; \text{discharging} \end{cases} \quad (5)$$

with

$$P_{eq} = P_{atm} * \exp\left(\frac{\Delta H}{RT} - \frac{\Delta S}{R}\right) \quad (6)$$

Two material pairs have preliminary been selected and each MH has been modeled separately to evaluate the behavior in terms of temperatures, composition and pressure, under selected operating conditions

For the first MH pair (Mg_2FeH_6 - TiFeH_2) kinetics data are available from SRNL experiments carried out for discharge at 500 °C and 1 bar. Uptake data for the

HTMH material are available in the literature [13] (uptake data at 623 K and 40 bar). In addition, (as previously shown) the discharge activation energy has been calculated at SRNL from a Kissinger plot. The available data have been fit using the kinetics expression reported in Equation 3, resulting in the kinetics parameters reported below.

Fast kinetics expressions (with uptake/discharge rates similar to LaNi_5) have been adopted for the LTMH material with the parameters reported below:

Table 10: Kinetics parameters of Mg_2FeH_6 - TiFeH_2 couple (Couple1)

	Mg_2FeH_6	TiFeH_2
Ca (1/s)	10000	65
Ea (J/molH ₂)	63000	21170
Cd (1/s)	12000	15.57
Ed (J/molH ₂)	90000	16420
X _M (molH ₂ /m ³)	32468	24600
X _m (molH ₂ /m ³)	0	0
ΔH (J/mol)	-77000	-28000
ΔS (J/mol/K)	-137.	-106

The second couple (NaMgH_2F - Na_3AlH_6) has been chosen since it represents one of the most promising MH based TES systems with the potential of approaching and reaching the ultimate targets. NaMgH_2F kinetics data are available from SRNL and Curtin University, for uptake at about 400 °C and hydrogen pressure of 40 bar (SRNL) and 491 °C and about 50 bar (Curtin University). In addition, (as shown in the other sections of the report) the discharge activation energy has been calculated from Kissinger plot, equal to 151500 J/mol. The available data have been fit using the kinetics expression (Equation 3). The LTMH material (Na_3AlH_6) properties have been shown in the other sections of the report with additional data available from previous studies carried out at SRNL [14]. Kinetics parameters have been evaluated from the last uptake experiments carried out at SRNL, reported in the current document, at 150 °C and hydrogen pressure of 30 bar. The activation energy values were assessed from a Kissinger plot with good agreement with values reported in previous studies [14]. Kinetics parameters for the coupled materials are reported in Table 11. A comparison between kinetics data and model predictions for NaMgH_2F at two different temperatures and pressures (experimental data from SRNL and Curtin University) is reported in Figure 29.

Table 11: Kinetics parameters of NaMgH_2F - Na_3AlH_6 couple (Couple2)

	NaMgH_2F	Na_3AlH_6
Ca (1/s)	120000	8E+5
Ea (J/molH ₂)	102500	70000
Cd (1/s)	1000000	5E+12
Ed (J/molH ₂)	151500	118600
X _M (molH ₂ /m ³)	32468	5400
X _m (molH ₂ /m ³)	0	0

ΔH (J/mol)	-96800	-47000
ΔS (J/mol/K)	-138.0	-134.9

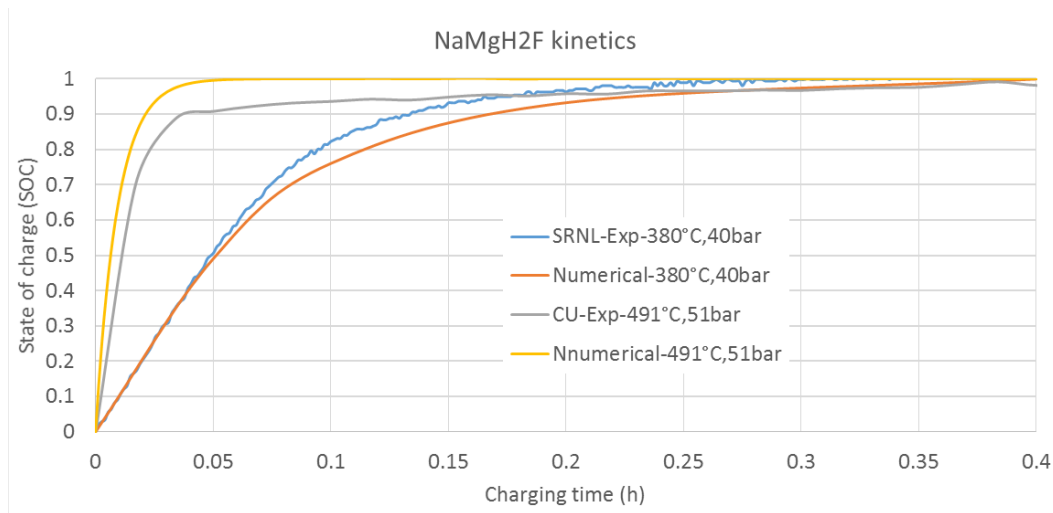


Figure 29: NaMgH₂F kinetics comparison between experimental and modeling data (experimental data provided by Curtin University)

Simulation conditions

The reactor geometry has been defined based on the experimental reactor currently available at SRNL. A 3D diagram of the reactor is shown in Figure 30, with the corresponding 2D axial symmetric diagram.

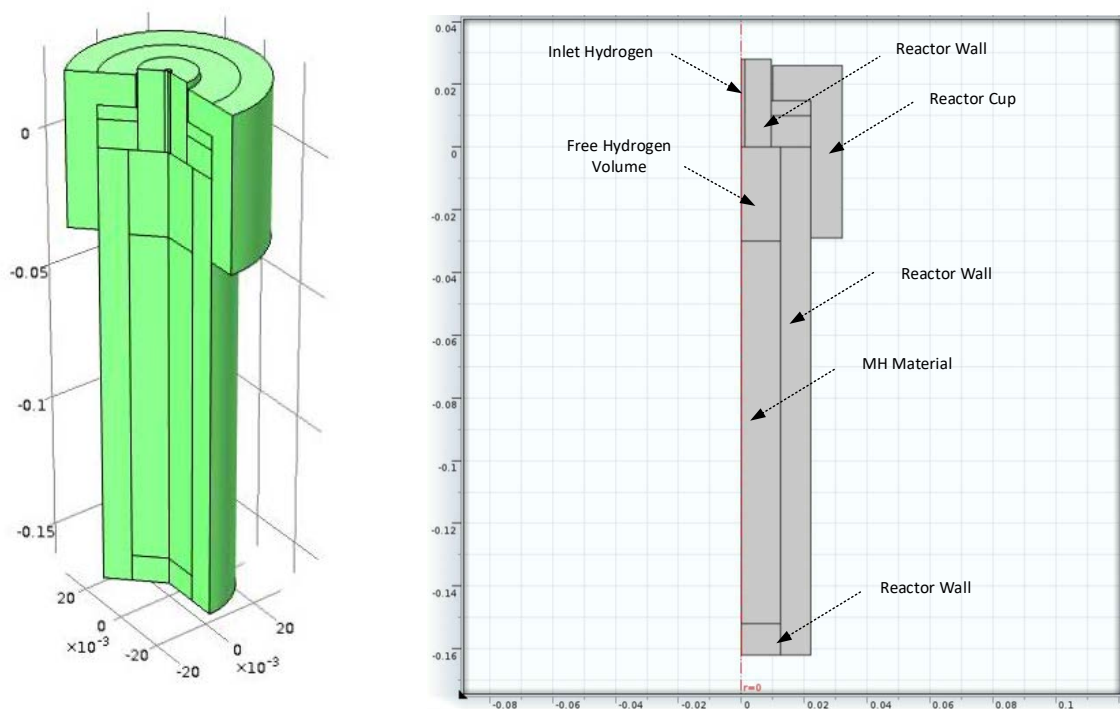


Figure 30: Reactor geometry (3D geometry and corresponding 2D axial symmetric geometry in COMSOL® Multiphysics)

Three positions were selected inside the reactor to collect the temperature, concentration and pressure data. These points are reported in the Figure 31. Pressure data points are P1 (0.005, -0.05), P2 (0.005, -0.09) and P3 (0.005, -0.13). Temperature and concentration data points are TC1 (0, -0.09); TC2 (0.005, -0.09) and TC3 (0.01, -0.09). The initial conditions to integrate the equations have been assumed as reported in the Table 12.

Table 12: Initial conditions for H₂ uptake in the MH beds

	Mg ₂ FeH ₆	TiFeH ₂	NaMgH ₂ F	Na ₃ AlH ₆
Initial T (K)	613	300	750	400
Initial P (bar)	3.9 (eq)	4.6 (eq)	2.9 (eq)	8.1 (eq)
Initial vel (m/s)	0	0	0	0
Initial c (mol/m ³)	25000	13000	14935	1000
Initial $\partial c/\partial t$ (mol/m ³ s)	0	0	0	0

Boundary conditions have been chosen according to the experimental conditions and to the material properties. Adiabatic conditions have been assumed for the HTMH reactor walls. The LTMH wall thermal condition has been set assuming a constant temperature (e.g. equal to 400 K for Na₃AlH₆). Inlet hydrogen temperature has been assumed equal to 300 K to simulate the real experimental conditions of the reactor. A “sigmoidal” inlet velocity profile with velocity values from 0 (at t=0 s) to maximum speed (achieved at t=60 s) has been assumed as the inlet condition to integrate the momentum balance equation.

Hydrogen uptake results for the Couple2 MH materials (NaMgH₂F and Na₃AlH₆) are reported in the following figures. The document reports only the results obtained for the Couple2 materials since this material pair is more promising in terms of potential to achieve the targets and are newly developed materials. Figures 32-33 report temperature profiles for hydrogen uptake for the pair of metal hydrides in the second MH couple (NaMgH₂F- Na₃AlH₆)⁵. And Figure 34 shows the uptake state-of-charge (SOC) for the same MH couple.

⁵ Concentration and pressure profiles have been omitted for brevity, but can be found in the Period 2 Continuation Report.

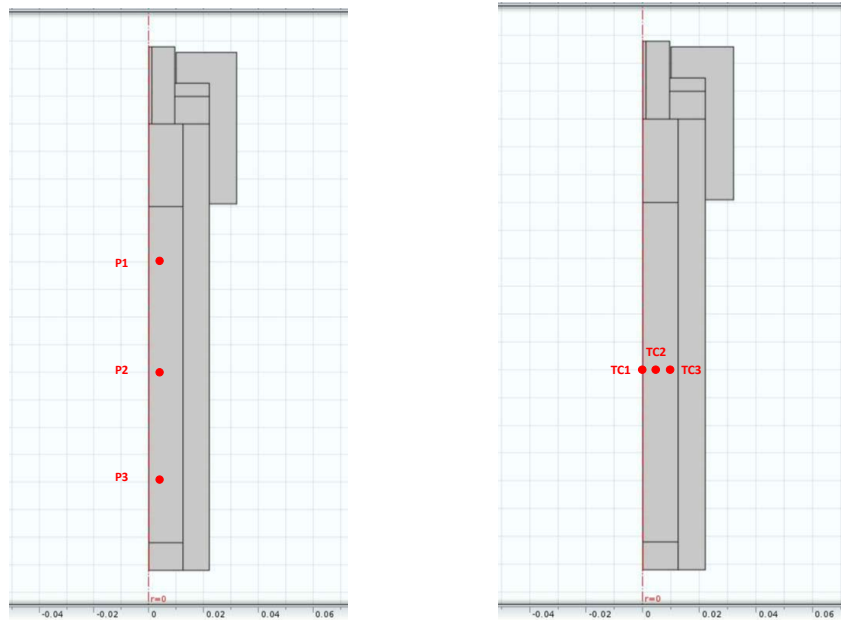


Figure 31: Pressure data points (P1, P2, P3) and temperature and composition data points (TC1, TC2, TC3)

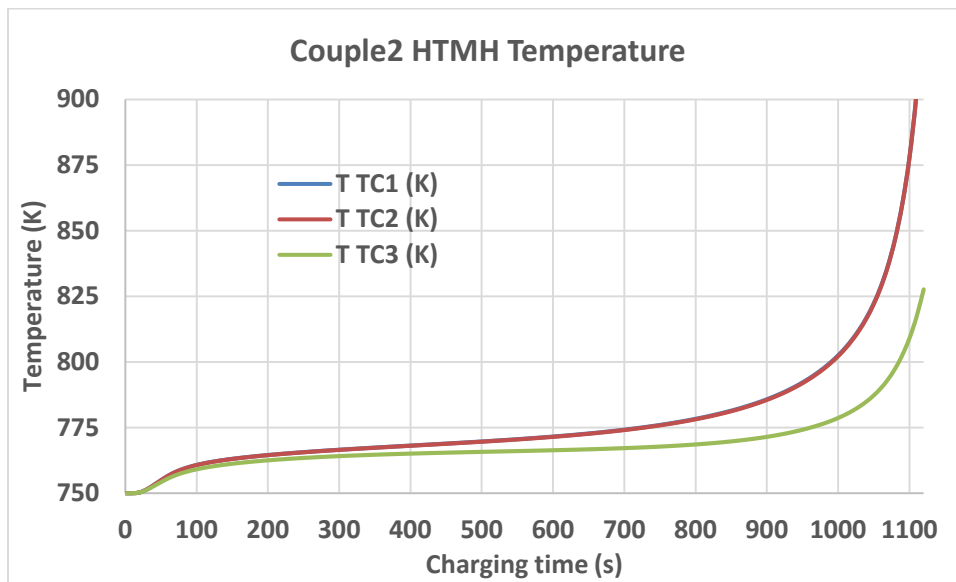


Figure 32: Temperature profile of NaMgH₂F MH bed during charging

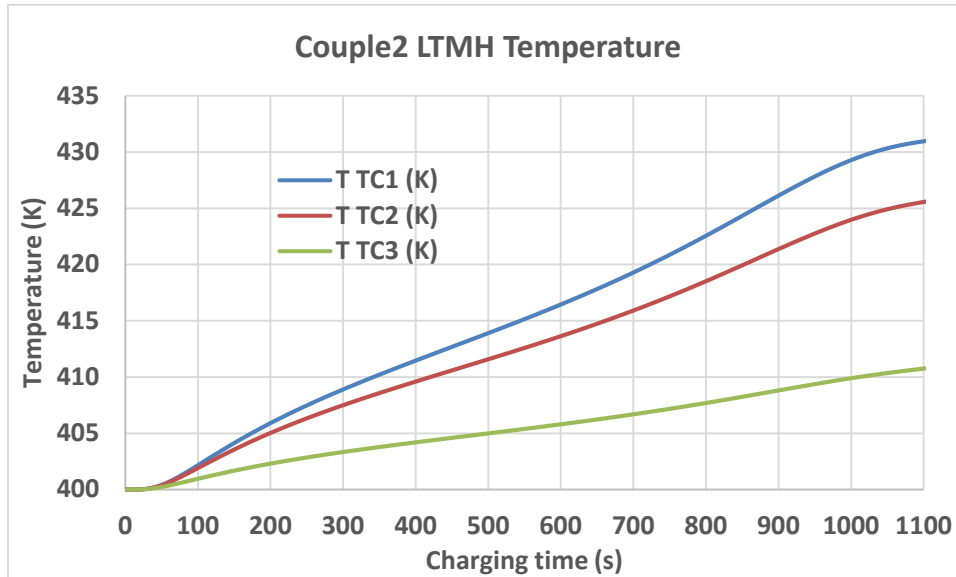


Figure 33: Temperature profile during Na_3AlH_6 MH bed H_2 charging

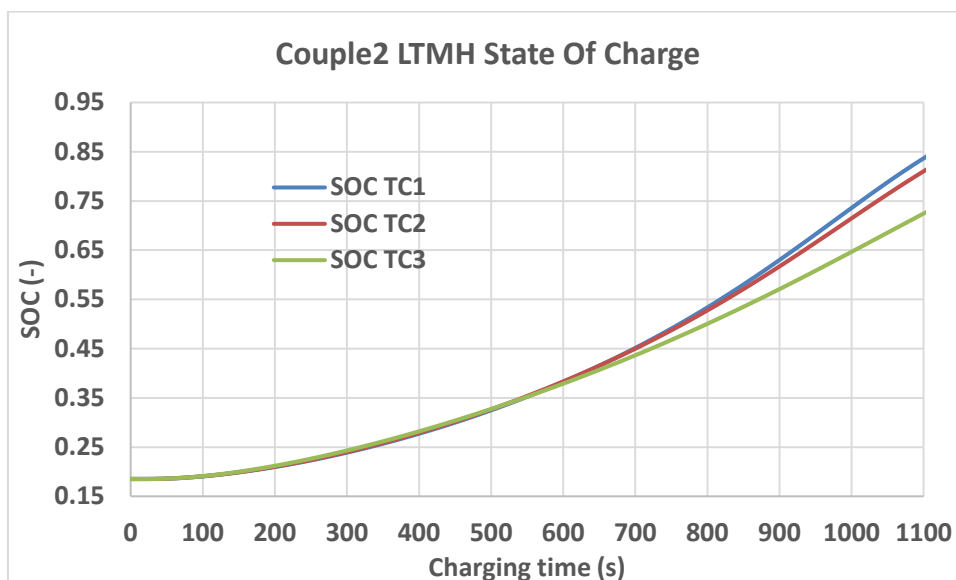


Figure 34: State Of Charge (SOC) during Na_3AlH_6 MH bed H_2 charging

Under the initial and boundary conditions assumed for the current analysis three different regions can be seen during the charging process of the HTMH. The first part (0-60 s) sees an increasing inlet hydrogen flow rate becoming constant (max flow rate) at about 60 s. The second region (up to 900-1000 s) sees hydrogen uptake at almost constant pressure. The third charging region sees a deep increase of the pressure inside the material with corresponding additional hydrogen uptake and temperature increase. As previously mentioned, for the Na_3AlH_6 material a constant T of 400 K has been assumed at the reactor wall. Accordingly, the results show: (1) lower thermal gradients inside the material (most of the heat during the hydrogen

charging process is exchanged with the external environment being at constant T of 400 K); (2) consequent more uniform SOC inside the material.

Several analyses have also been carried out for hydrogen discharging, both for HTMH and LTMH materials. As an example, results for Couple2 HTMH (NaMgH₂F) are reported in Figure 35 showing temperature profiles⁶. The initial conditions are reported in Table 13.

Table 13: Initial conditions for H₂ discharge in the NaMgH₂F MH bed

	NaMgH ₂ F
Initial T (K)	823
Initial P (bar)	11.6 (eq)
Initial vel (m/s)	0
Initial c (mol/m ³)	29900
Initial $\partial c/\partial t$ (mol/m ³ -s)	0

The discharging procedure sees a (outlet) pressure reduction (in 100 s) from the initial equilibrium value (11.6 bar) down to 0.12 bar (value assumed equal to 1% of the initial equilibrium pressure) and a (wall) temperature increase (in 100 s) from the initial value (823 K) to 948 K (equal to 675 °C).

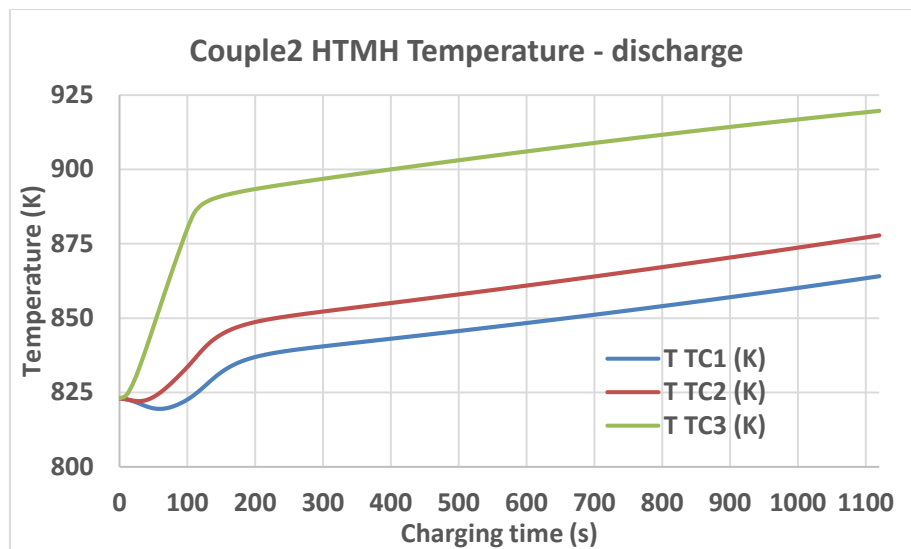


Figure 35: Temperature profile of NaMgH₂F MH bed during hydrogen discharging

As part of the work carried out during Period 3, the MH bed reactors have been paired with H₂ gas reservoirs to assess the performance of charging and discharging of the MHs, paired with hydrogen gas tanks. A 3D sketch of the overall system is shown in Figure 36, with the corresponding 2D axial-symmetric adopted to model the system.

⁶ Concentration and pressure profiles can be found in Period 2 Continuation Report.

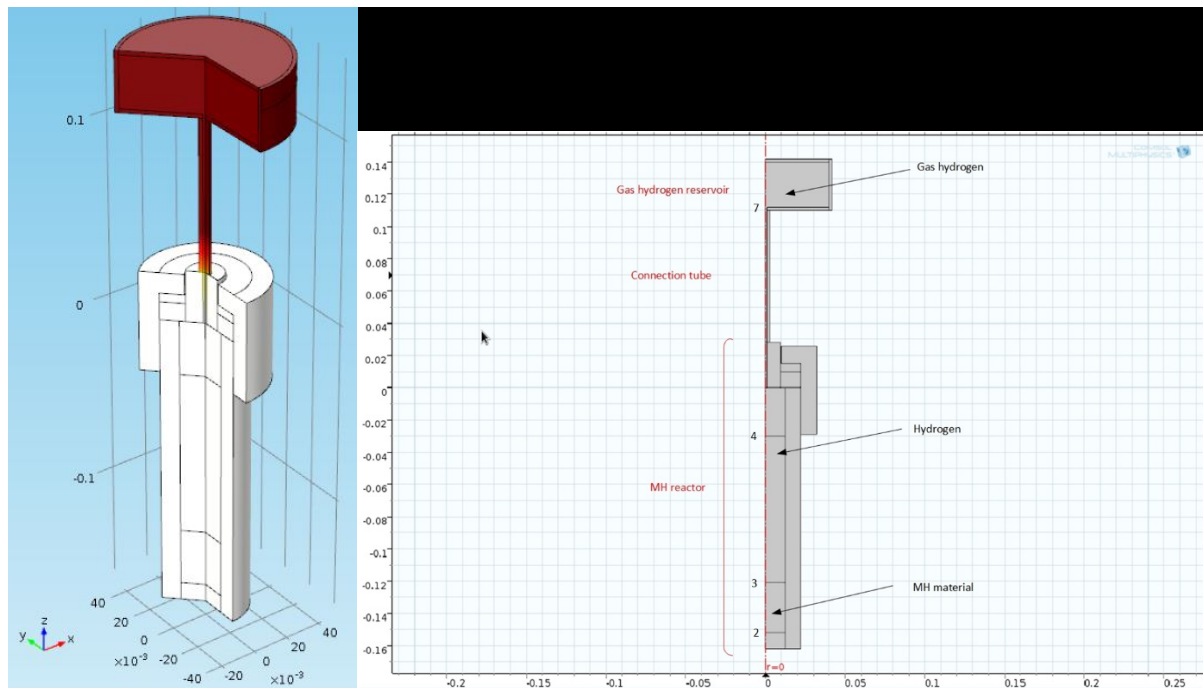


Figure 36: MH reactor coupled with a gaseous hydrogen reservoir – 3D model geometry with corresponding 2D model axial-symmetric geometry

Four cases have been simulated, with charging and discharging of the HTMH and LTMH materials coupled with the reservoir. For brevity this document contains the results obtained only for the HTMH (Mg-Fe material) discharging. For this case the following initial conditions (Table 14) have been adopted, according to the experimental set up.

Table 14: Initial conditions of the MH reactor coupled with gaseous hydrogen tank (as in Figure 36)

	Mg_2FeH_6
Initial MH T (K)	723
Initial gas H_2 reservoir T (K)	293
Initial P (bar)	0.1
Initial vel (m/s)	0
Initial State Of Charge (SOC)	90%
Initial $\partial c/\partial t$ (mol/m ³ -s)	0

The boundary conditions of the model have been set according to the experimental conditions: a fixed temperature of 723 K has been assumed for the reactor body boundary condition, adiabatic conditions have been assumed for the head of the MH reactor and convective heat transfer condition has been assumed for the tubing and gas reservoir. The data for temperature, pressure and SOC of the MH have been collected. Figure 37 shows the SOC profile assessed at point 3 (see Figure 36). Figure 38 and 39 show pressure and temperature profiles in the reactor. With the given boundary conditions a peak temperature reduction can be observed (inside the MH material) during initial discharging of the MH from 0.1 bar up to about 3-5 bar. This is due to the very fast reaction rate at the beginning of discharging, when the external pressure is about vacuum pressure.

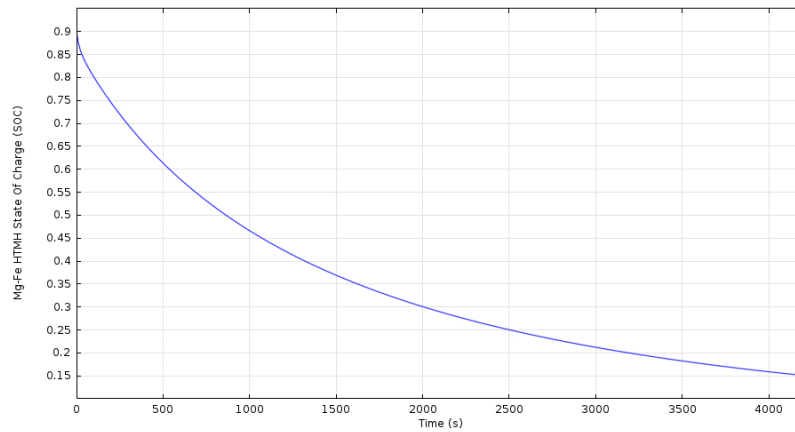


Figure 37: SOC of the MH material evaluated at point 3 (Figure 37)

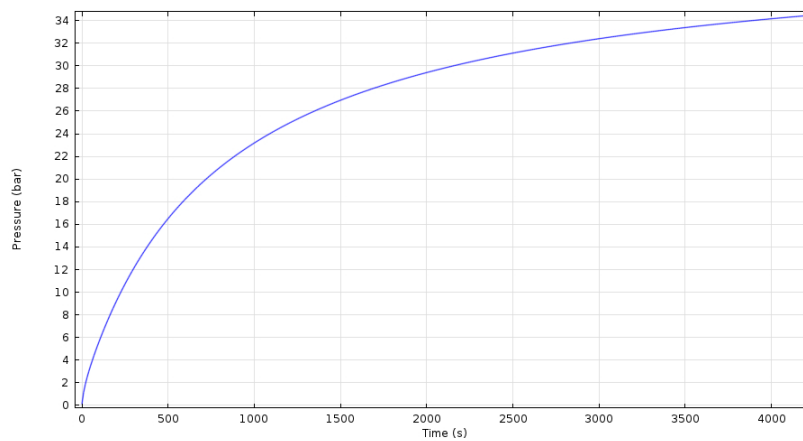


Figure 38: Pressure profile during the discharging of the MH material.

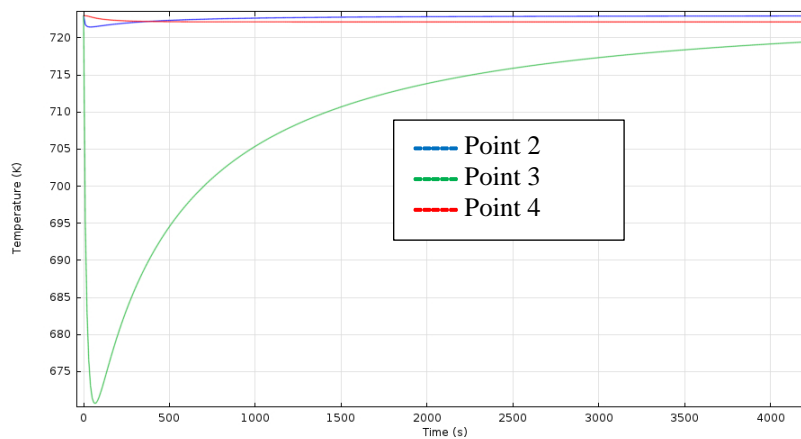


Figure 39: Temperature of the MH material at points 2, 3, 4 (Figure 36)

Additional results are reported here for model validation, comparing numerical results with experimental results for the Na_3AlH_6 LTMH material. A new reactor has been adopted to simulate (numerically and experimentally) the system, allowing easier and more precise thermocouple placement and pressure measurement compared to the previous reactor.

The volume of the new reactor is $3.9 \times 10^{-6} \text{ m}^3$, containing 2 g of Na_3AlH_6 material at a density of 517 kg/m^3 , without any material compaction in the current configuration.

Simulation conditions

The reactor geometry has been defined based on the new experimental reactor currently available at SRNL. A 3D diagram of the new reactor is shown in Figure 40, with the corresponding 2D axial symmetric diagram.

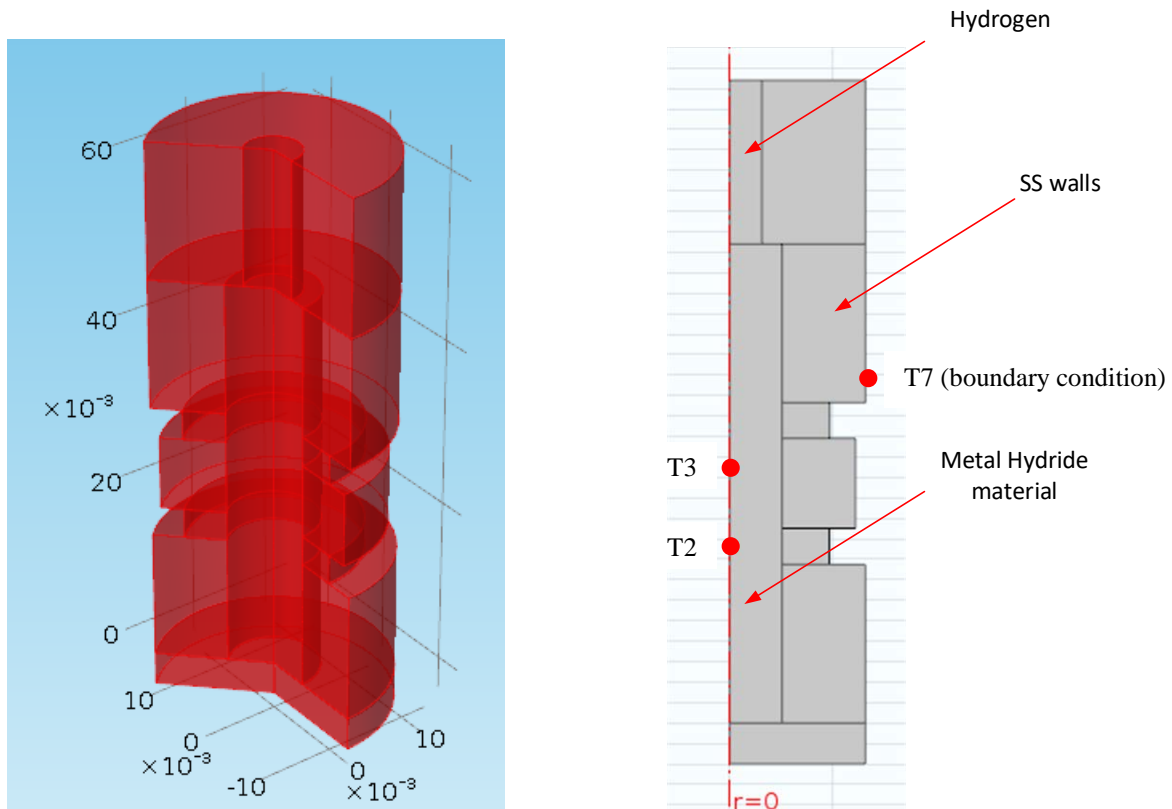


Figure 40: Reactor geometry (3D geometry and corresponding 2D axial symmetric geometry in COMSOL® Multiphysics)

Two positions were selected inside the reactor to collect the temperature, concentration and pressure data. Data points are T2 ($r=0.00$, $z=0.0175$), T3 ($r=0.00$, $z=0.0245$). The initial conditions to integrate the equations have been assumed as reported in the Table 15, based on the adopted experimental conditions.

Table 15: Initial conditions for H_2 uptake in the MH bed

	Na_3AlH_6
Initial T (K)	440
Initial P (bar)	1.1
Initial vel (m/s)	0
Initial c (mol/m ³)	38.8 (equilibrium)
Initial $\partial c/\partial t$ (mol/m ³ s)	0

Boundary conditions have been chosen according to the experimental conditions. A heater was wrapped around the reactor to keep the wall temperature approximately constant. The wall temperature has been measured (T7 position) during the

experimental activities and the values have been used as temperature wall boundary condition. The inlet hydrogen temperature has been assumed equal to 300 K. The pressure inlet condition has been included based on the data measured during the experiments and reported in Figure 41. Hydrogen uptake results for the Na_3AlH_6 are reported in the following figures.

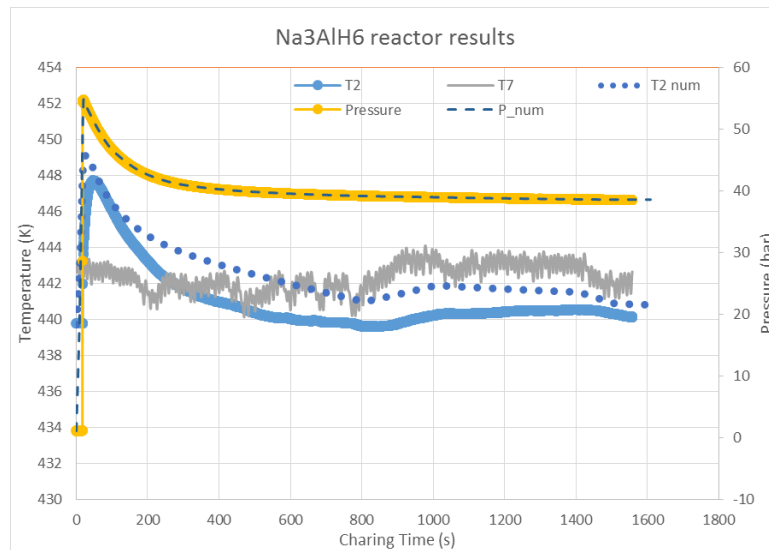


Figure 41: Temperature and pressure profiles at the locations shown in Figure 41. Numerical and experimental results are shown

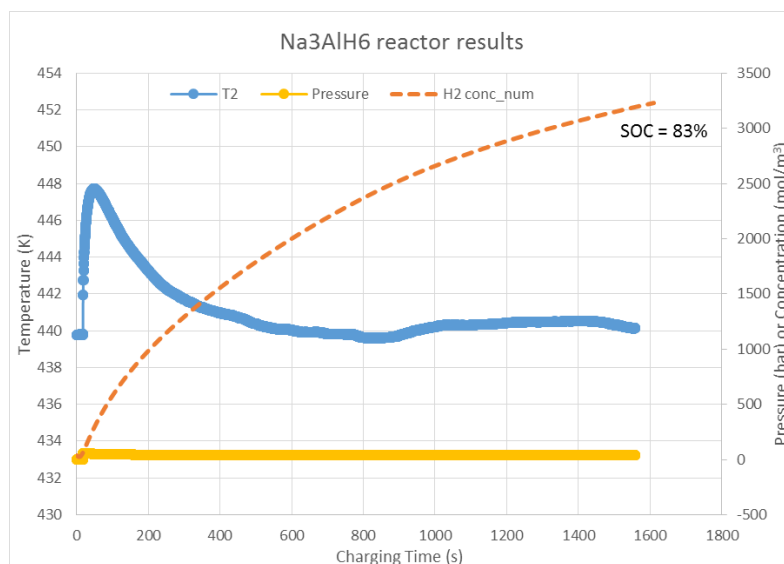


Figure 42: Hydrogen concentration profile at the locations shown in Figure 14.

In general, good agreement between numerical and experimental results has been found as reported in Figure 42. In particular, the model reproduces the temperature profile well in terms of derivatives of the temperature function, demonstrating that the different phenomena are well represented (e.g. pressure variation). After about 30 minutes of hydrogen charging the state of charge of the bed is approximately 83% (figure 42) under the conditions previously described. Due to the reactor configuration and the amount of material placed inside the reactor no appreciable temperature spatial gradients have been noticed inside the metal hydride material during the experimental activities (TC2 and TC3 values are comparable), with

confirmation from the modeling results. Results for the discharging process are available as well, with an agreement between experimental and numerical results on the same order of the charging case reported in Figure 41.

MH System models

The system model for the coupled metal hydride bed has been developed and has been integrated into the overall CSP plant system model developed in TRNSYS®. A sketch of the CSP is shown in Figure 43. The metal hydride based TES system model was initially developed during the last part of Period1. The model has been extensively revised, including first draft kinetics expressions for the newly developed materials. When additional data are available for the new materials, suitable more precise and refined kinetics will be included for the other new developed materials as well. In addition, SRNL developed a CSP plant model in TRNSYS® based on available models developed by German Aerospace Center (DLR) and suitably modifying them for the current application.

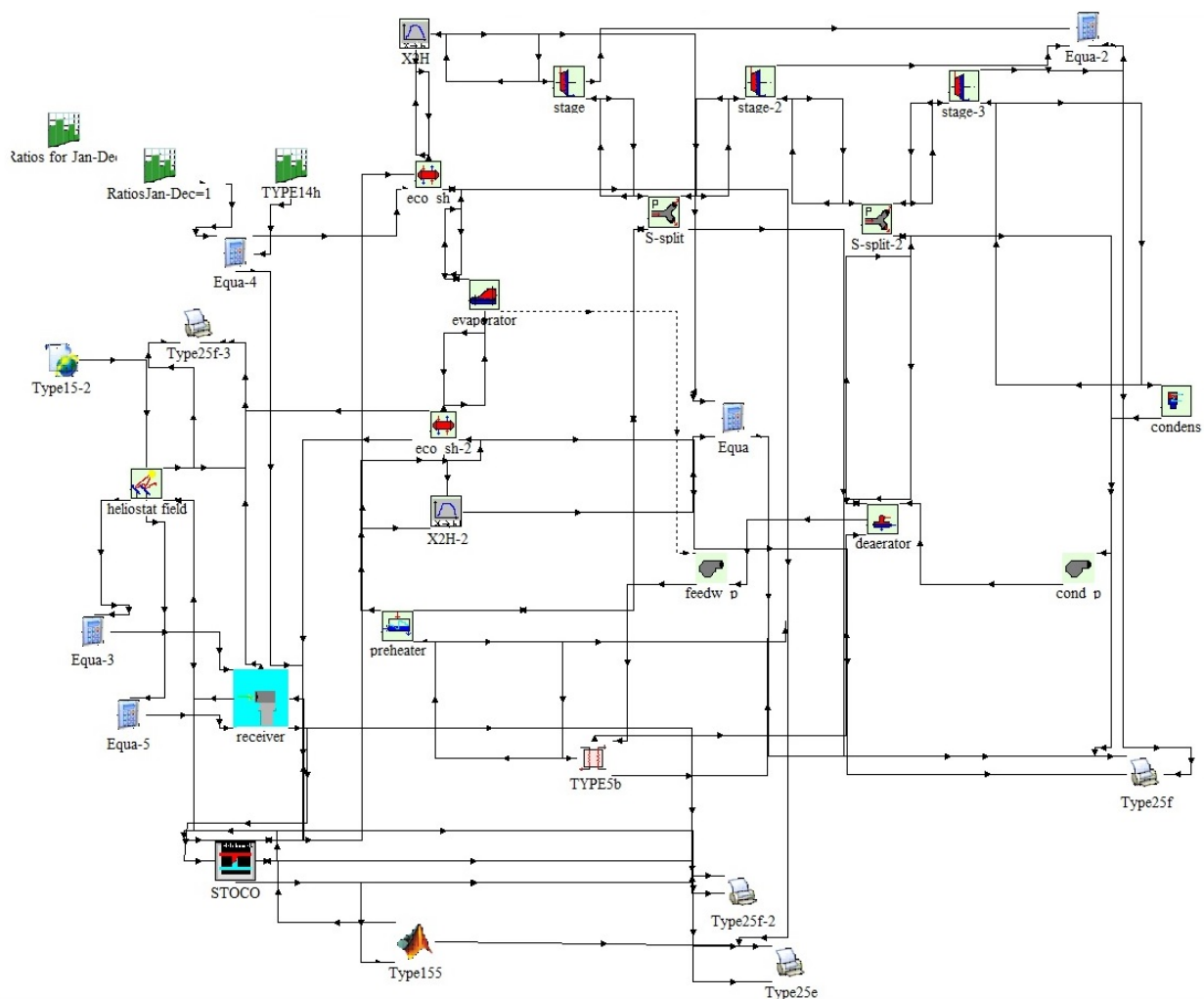


Figure 43: CSP plant model sketch in TRNSYS®.

The CSP plant model and conditions

The power plant (PP) section is based on a Hirn cycle with the following properties, briefly summarized in Table 16. The PP has been assumed working at nominal conditions from 7 am to 7.30 pm during the day, thus achieving a PCF of around 50%.

Table 16: Hirn power plant main properties

Steam pressure (bar)	160
Maximum steam temperature (°C)	630
Condenser pressure (bar)	0.05
Number of steam extractions	2
First extraction pressure (bar)	52.3
Second extraction pressure (bar)	8.5
Degasifier pressure (bar)	8.5
Out thermal power (MW)	195
Cycle efficiency (%)	39.1

The assumed weather scenario is that of Phoenix (AZ), with conditions available and already included in the extended TRNSYS® database (Type15-2 in Figure 44). The MH based TES system model has been developed in Matlab® and included in the CSP system ('Type155' in Figure 43). The storage system is interfaced with the other CSP equipment through the Storage Control unit (STOCO in Figure 43) which elaborates the inlet/outlet conditions of the storage system, the storage system conditions at the interface with the solar receiver (solar receiver HTF flow rate, inlet temperature and outlet temperature) and the storage system conditions at the interface with the power plant (steam generator HTF flow rate, temperature and pressure). The STOCO unit provides the TES system with the following 4 inputs (from the STOCO to the TES): HTF mass flow rate (kg/h) during heat storage; inlet temperature of the HTF (°C) during heat storage; HTF mass flow rate (kg/h) during heat release from the TES; inlet temperature of the HTF (°C) during heat release from the TES. The TES system in turns provides the STOCO unit with the following 3 outputs (from the TES to the STOCO): the outlet temperature of the HTF (°C) during heat storage; the outlet temperature of the HTF (°C) during heat release from the TES; the heat stored (MJ) in the TES unit.

The MH system model

The MH based TES system model was developed as part of the Period 1 activities. Selected material pairs have been modeled, adopting the kinetics expression reported in Equation 3. The previously developed models (in Mathcad®) were transposed into Matlab® code. The Matlab® code used an input file for the bed parameters, as well as providing links to external program calls to pass time dependent information to an external program (TRNSYS®). The Matlab® code uses an ordinary differential equation (ODE) solver to evaluate the coupled bed equations. The model takes into account the thermal capacity of the bed, hydrogen properties, as well as pressure effects.

With the power plant conditions given in Table 15, the most promising candidate materials are TiH₂ and NaMgH₂F, to be paired with TiFeH₂ or Na₃AlH₆ material. For the present system, a 20-day simulation was conducted. The thermal input to each bed was assumed equal to the maximum thermal power stored/released during the year (equal to 352.7 MW corresponding to a thermal storage of 13 hours at

maximum solar power). The thermal input was switched every 12 hours to simulate a daytime (heat storage)/nighttime (heat release) cycle. Results of the simulation carried out for the TiH_2 - TiFeH_2 pair are reported in Figures 44-45 for a 20-day simulation.

The beds are initialized to 95% full for HTMH material bed (bed1) and 5% full for LTMH material bed (bed 3). The initial temperature for each of the bed is calculated as the equilibrium temperature at 3 bar (initial assumed pressure).

A pressure transient profile can be seen in Figure 44⁷. The pressure fluctuation of the bed system is less than 0.1 bar between the day and night cycle. The temperature profiles for the beds can be seen in Figure 45⁸. The bed temperatures vary slightly between a day and night cycle with a slight trend of increasing average bed temperature over the course of the 20-day cycle.

Additional material pairs have been simulated. One of the most promising materials, as previously described in the document, is NaMgH_2F . The TES system based on NaMgH_2F - TiFeH_2 couple has been assumed as the baseline system and has been integrated in the CSP plant model (shown in Figure 43).

The NaMgH_2F tank has been conceptually designed assuming the SunShot targets with the properties reported in the previous reports. Under these conditions the volume of the HTMH is about 8600 m^3 (mass of approximately 12000 tons) with a mass of hydrogen stored in the bed of about 340 tons. This TES system has been included in the CSP plant and simulated, with the results shown in the next sections.

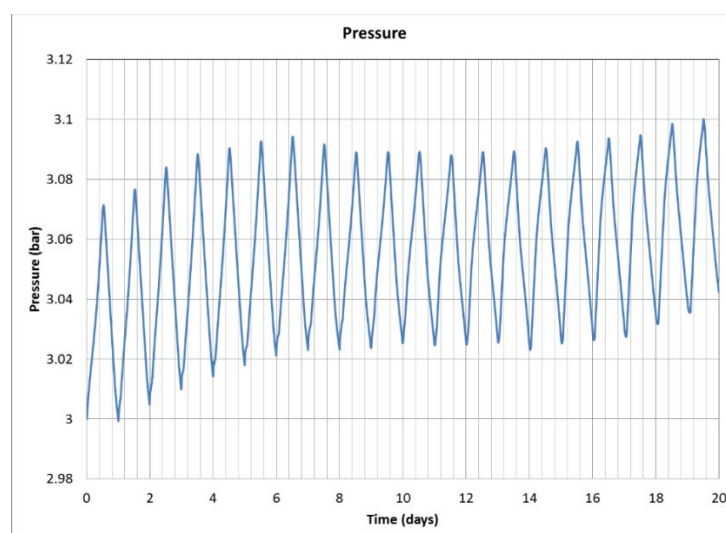


Figure 44: Coupled Bed (TiH_2 – TiFeH_2) Pressure Profile

⁷ IN this case the pair TiH_2 – TiFeH_2 has been selected

⁸ Idem as 8

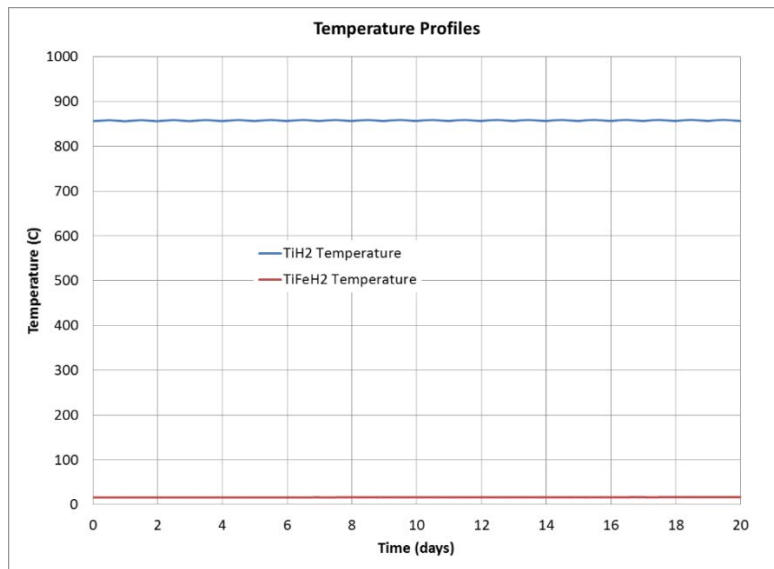


Figure 45: Coupled Bed (TiH₂ – TiFeH₂) Temperature Profiles

The CPS plant model results

Due to the operating conditions of the CSP plant, the NaMgH₂F-TiFeH₂ pair has been selected to be the TES system. The simulation was carried out considering the charging/discharging of the TES system for 7 days (168 hours) during March under the operating and site conditions previously described. The results report the cycling ability of the TES system included in the overall CSP plant.

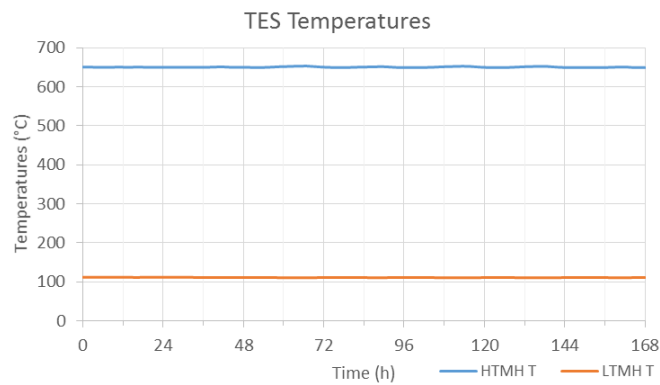


Figure 46: Temperatures of the two MH tanks (HTMH: NaMgH₂F; LTMH: TiFeH₂)

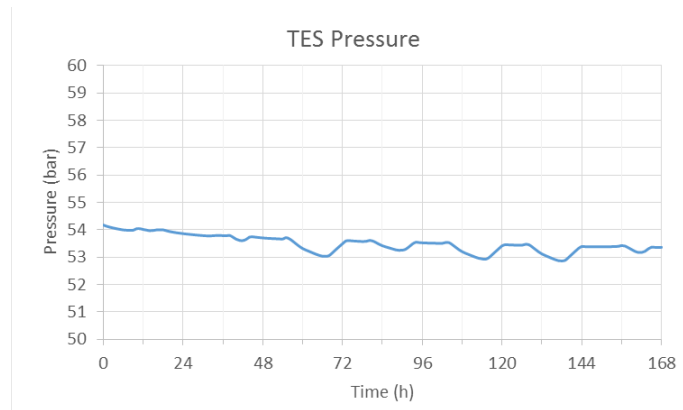


Figure 47: Pressure of the TES system

The temperatures of the two MH material tanks in the TES system (as shown in Figure 46) remain almost constant throughout the storage time, with the operating HTMH bed temperature at about 651 °C. The pressure of the TES system is almost constant as well, as reported in Figure 47.

2.3 Design and Testing of a Bench-Scale MH TES System

A bench-scale cycling system was fabricated for the pairing of a LTMH to a HTMH. The layout of the instrument is shown in Figure 48 below. This cycling system was developed to provide experimental data for modeling purposes and to demonstrate the pairing of two metal hydride beds for TES applications.

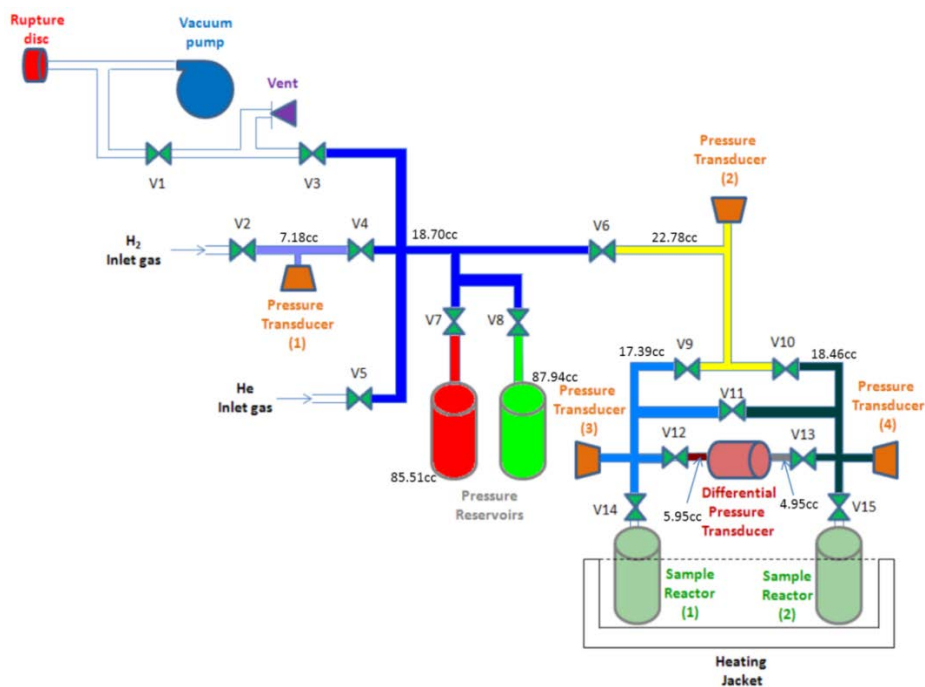


Figure 48: Schematic of the system that will be utilized for the bench scale testing of selected metal hydride pairs including the calibrated volumes for each section of tubing and reservoir.

2.3.1 Design and Fabrication of a Bench-Scale MH TES System

An automated bench scale cycling system was constructed from an array of pneumatic valves, tubing, heaters, pressure transducers, electronics, and high temperature reaction vessels. A LabVIEW® program was written to provide computer control over the cycling apparatus. The system was designed to measure pressures in various sections of the instrument to allow for the quantification of hydrogen being moved between the two metal hydride beds. The LabVIEW® control panel is shown below in Figure 49. The full bench scale system and reaction vessels can be seen in Figures 50 and 51.

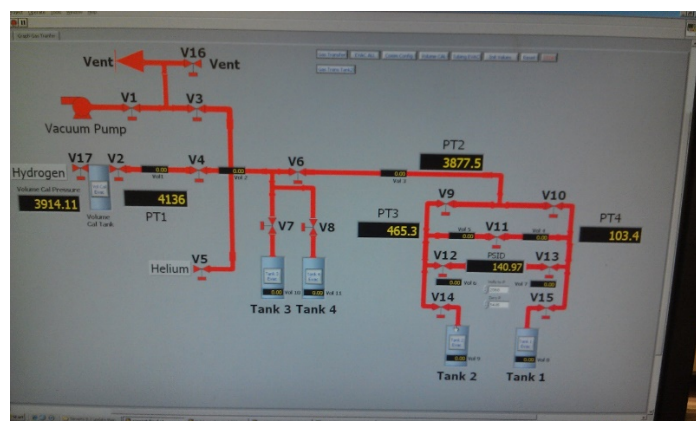


Figure 49: Software control panel for the bench-scale cycling apparatus.

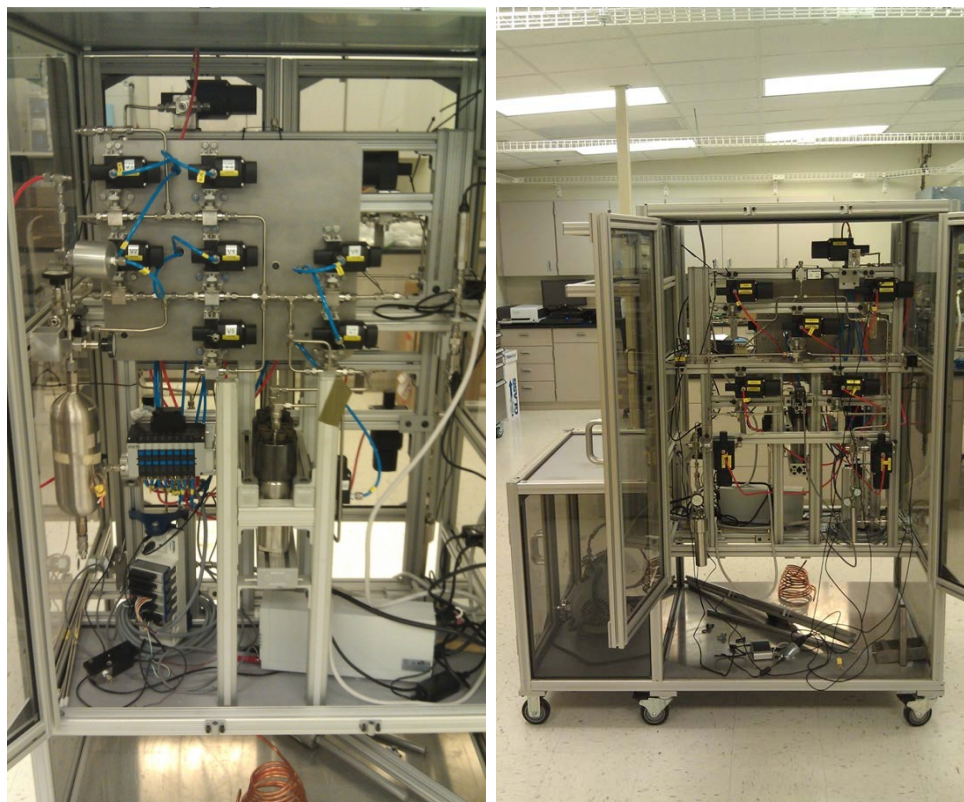


Figure 50: Full view of the bench-scale hydride bed cycling system.

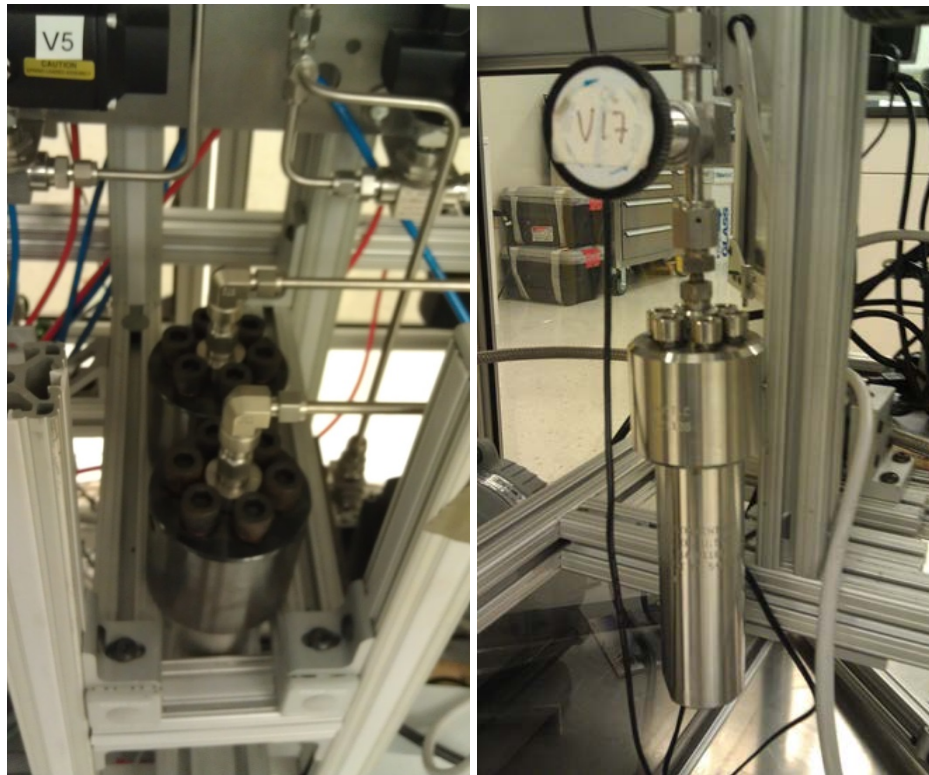


Figure 51: Hydrogen pressure reservoirs (left) and metal hydride reaction vessel (right) to be used in the bench scales system.

2.3.2 Operation of a Bench-Scale MH TES System

The bench-scale metal hydride system's volumes were calibrated and the overall system tested for operation. The automated volume calibration software developed was determined to be highly reproducible and consistent with the volumes obtained by other methods. The independent cycling of the metal hydride materials Na_3AlH_6 and Mg_2FeH_6 have been carried out manually and demonstrated that the system is suitable for operation. To quantify the exact amount of hydrogen being transferred from one hydride bed to the other, a batch method was required initially. This involves dehydrogenating one hydride bed into a reservoir volume, followed by isolation of the desorbing bed and introduction to the absorbing hydride bed. To qualitatively demonstrate the heat generated from the hydrogenation of Mg_2FeH_6 , the dehydrogenated material was introduced to 25, 50, and 100 bar of H_2 at $\sim 330^\circ\text{C}$ as shown in Figure 52. As shown a dramatic increase in temperature (thermocouple located in the sample) is observed. Since this heating system is based on a feedback thermocouple to remain at constant temperature and not constant power, the heater shut off once the target temperature is exceeded. To quantify heat a constant power heater and excellent insulation is required.

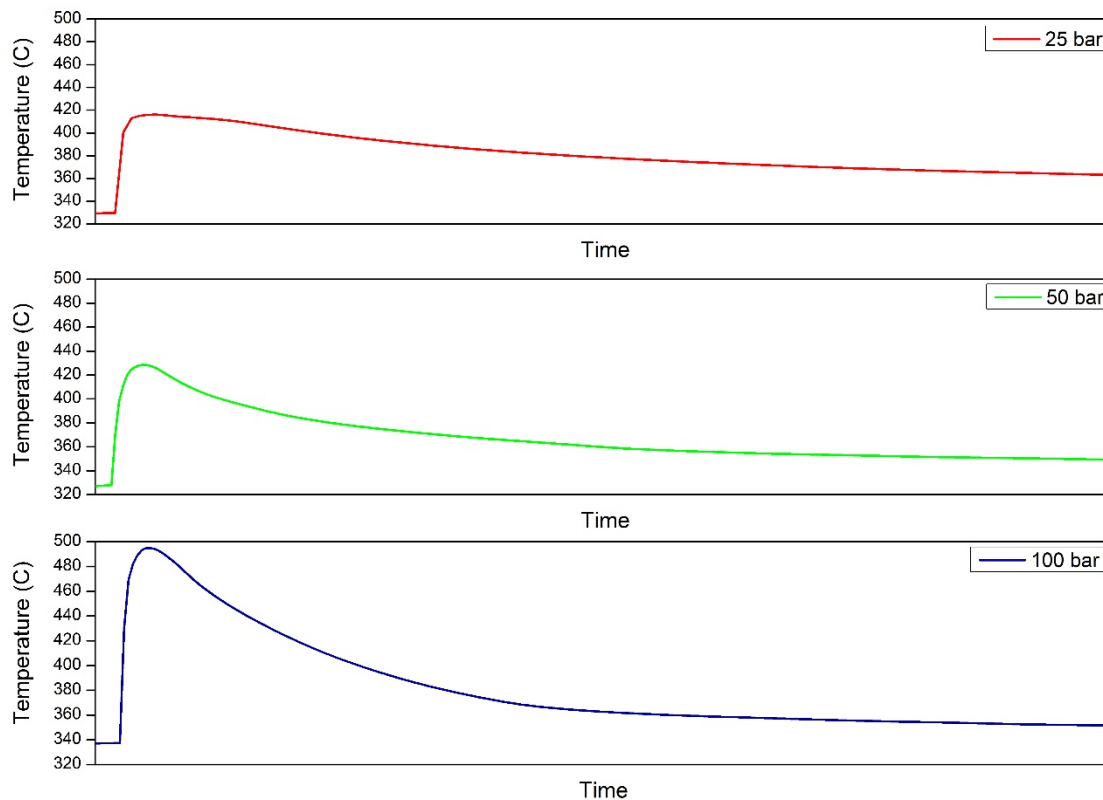


Figure 52: Temperature of Mg_2FeH_6 during hydrogenation at various pressures to demonstrate heat generation.

3.0 Project Summary and Conclusions

SRNL and its partner CU have proposed and demonstrated the viability of employing metal hydrides for storing thermal energy for CSP applications. Initial material characterization and screening analysis showed that while many existing material candidates could meet many of DOE's SunShot TES targets, none of the existing materials could meet all of the DOE targets, specifically low system cost at high temperatures. SRNL and CU began an aggressive program to identify materials that could be modified to enhance their operating temperature but still be low cost. This program led to several promising new candidate materials, one in particular based on Ca-Si was patented by SRNL for this application and shown to operate at very high temperatures ($>650^{\circ}C$) and still be low cost. The engineering properties of this material were obtained and then employed in a series of screening, transport and system models to evaluate the performance and cost of this new material for TES applications. A bench-scale metal hydride TES system was built, tested and evaluated to demonstrate HTMH and LTMH paired operation and performance which is a key to the viability of a metal hydride based TES system.

3.1 Milestones and Accomplishments

Material Development, Characterization and Performance

- Low temperature metal hydrides based on sodium alanates were investigated to pair with a suitable high temperature metal hydride for CSP TES

applications. It was discovered that Na_3AlH_6 with additives including expanded natural graphite and aluminum metal performed the best. Although the hydrogen capacity of the Na_3AlH_6 is less than that of the NaAlH_4 , the cycle stability and pressure required for re-hydrogenation were found to be far superior.

- A variety of high temperature metal hydrides were investigated for TES applications. These include MgH_2 , Mg_2FeH_6 , NaMgH_3 , TiAl , NaMgH_2F , CaAl , CaAl_2 , and Ca_2Si . It was determined that Ca_2Si operated at very high temperature (750 °C), had a reasonable hydrogen capacity, and was very low cost.
- Thermal and kinetic properties of the previously mentioned materials were measured including enthalpy, entropy, bulk density, hydrogen capacity, activation energy, thermal conductivity, etc.
- A bench-scale cycling apparatus was built to demonstrate the cycling of hydrogen between the two hydride beds.
- Various high and low temperature metal hydride materials were cycled over 100 times to determine cycle stability.
- A low cost metal hydride capable of reversibly storing ~ 2 wt. % hydrogen at 750 °C was demonstrated for the first time. This material is currently most promising high temperature metal hydride material discovered for TES applications at high temperatures (> 650 °C) which is capable of meeting DOE cost targets.

Modeling

- A screening analysis tool was developed to evaluate the performance of the MH based TES system and to compare it against the targets. The screening criteria included: system cost, system exergetic efficiency, volumetric efficiency, operating temperature.
- A TES system model was developed to model the coupled MH pairs. The model is a lumped parameters transient model that incorporates mass and energy balance equations along with the kinetics of the two materials.
- A detailed Finite-Element based model was developed to evaluate the detailed behavior of the MH system, highlighting the gradients inside the reactor. The model is a multidimensional transient model, developed in COMSOL™, which includes mass, energy and momentum balance as well as the kinetics of the MH materials.
- The screening tool was used to evaluate various existing MH material systems resulting in 3 potential MH pairs, being able to approach the SunShot targets: (1) $\text{NaMgH}_3 - \text{NaAlH}_4$; (2) $\text{TiH}_2 - \text{TiFeH}_2$; (3) $\text{CaH}_2 - \text{TiFeH}_2$. Even if these materials are able to meet and exceed some of the targets, none of the screened pairs could meet all the targets. This required additional material development that resulted in three potential new high temperature MH materials (NaMgH_2F , TiAl based HTMH, CaSi based HTMH) showing improved performance.
- The modified materials were examined and their performance has been evaluated. Results showed that the CaSi based system can meet many of the targets and closely approach the other targets.
- A statistical cost methodology was developed and applied (as part of the Year 2 scope of work), showing that the CaSi based material can achieve a cost of ~16 \$/kWhth under selected conditions.

- An integrated TES system model was developed in MatLab® and was integrated into a Trnsys® program, to simulate the overall solar plant. Such a plant included a solar tower based receiver, a supercritical steam power plant (operating at about 620 °C) and the TES system, comprised of NaMgH₂F HTMH coupled with the TiFeH₂ LTMH material. Results showed that the coupled MH TES system can adequately be integrated in a solar steam power plant and can adequately work under different operating conditions.
- The detailed MH model was used to simulate the behavior of the selected modified LTMH material (Na₃AlH₆) and to compare the obtained results with the experimental results, showing very good agreement about the temperature and pressure profiles.
- As part of the Year 3 project scope of work, the MH pair MgFe₂H₆-Na₃AlH₆ has been examined and modeled using the previously developed system model. Results showed that the two materials can successfully be paired under selected experimental conditions and properties.

3.3 Path Forward

With DOE support during this 3-year project, SRNL has quickly become a world leader in this technology. SRNL has been granted a potentially transformational patent and had 6 peer-reviewed papers published in this area. With its partner CU, SRNL initiated an International Energy Agency (IEA) working group for MH TES technology and has helped create significant international research interest and excitement in this area. SRNL has also received considerable interest from several solar system design and installation firms, including United Sun Systems and Brayton Energy. SRNL has received additional funding to continue its MH TES development from Brayton Energy as well as through a special Laboratory Directed Research and Development Initiative.

4. References

- [1] R. Zidan, "Storing High Exergetic Thermal Energy Based on Reversible Alloying and High Enthalpy Hydrides", Patent Disclosure No. SRS-14-021, Provisional Patent Number 62/087,939 filed on 12/5/2014.
- [2] DOE's Hydrogen Storage Engineering Center of Excellence (HSECoE) website: hsecoe.srs.gov
- [3] Corgnale C, et al. *Ren Sustain Energy Reviews*, 38(2014) 821-833.
- [4] K. Bohmhammel., et al, *Thermochimica Acta*, 310, 1998, 167-171
- [5] F.C. Gennari., et al, *Journal of Alloys and Compounds*, 339, 261-267 (2002)
- [6] Felderhoff M, et al., 14th International Symposium on Metal-Hydrogen Systems. 20-25 July 2014, Salford (UK).
- [7] Ward P, et al., *Applied Physics A*, 2016, 122, 462.
- [8] Corgnale C et al., *Int J Hydrogen Energy*, under review
- [9] Sheppard D., et al *RSC Advances*, 2014,4,26552-26562.
- [10] Maeland AJ, et al *Int J Hydrogen Energy* 24, 163-168 (1999).
- [11] Ito K, et al *Acta Materialia* 2002, 50, 4901-4912
- [12] Corgnale C, et al, *IJHE* 37(3),2012,2812-2824
- [13] Li S et al, *Transactions of Nonferrous Metals Society of China* 20(2010) 2281-2288

- [14] Hardy B. 'Geometry, heat removal and kinetics scoping models for hydrogen storage systems' WSRC-TR-2007-00439, Revision 0, Savannah River National Laboratory, 2007